JOURNAL OF PETROLOGY | VOLUME 45 | NUMBER 5 | PAGES 975–1011 | 2004 | DOI: 10.1093/petrology/egh001

Geochemical Constraints for the Genesis of Post-collisional Magmatism and the Geodynamic Evolution of the Northern Taiwan Region

KUO-LUNG WANG[1,2]*, SUN-LIN CHUNG[1], SUZANNE Y. O'REILLY[2], SHEN-SU SUN[3], RYUICHI SHINJO[4] AND CHANG-HWA CHEN[5]

[1]DEPARTMENT OF GEOSCIENCES, NATIONAL TAIWAN UNIVERSITY, PO BOX 13-318, TAIPEI 106, TAIWAN

[2]ARC NATIONAL KEY CENTRE FOR THE GEOCHEMICAL EVOLUTION AND METALLOGENY OF CONTINENTS (GEMOC), DEPARTMENT OF EARTH AND PLANETARY SCIENCES, MACQUARIE UNIVERSITY, SYDNEY, N.S.W. 2109, AUSTRALIA

[3]16 GIFFEN CLOSE, HOLT, CANBERRA, A.C.T. 2615, AUSTRALIA

[4]DEPARTMENT OF PHYSICS AND EARTH SCIENCES, UNIVERSITY OF THE RYUKYUS, OKINAWA, JAPAN

[5]INSTITUTE OF EARTH SCIENCES, ACADEMIA SINICA, PO BOX 1-55, NANKANG, TAIPEI, TAIWAN

RECEIVED NOVEMBER 14, 2002; ACCEPTED OCTOBER 21, 2003

Taiwan is an active mountain belt created by the oblique collision of the northern Luzon arc with Asia. Late Pliocene extensional collapse of the northern Taiwan mountain belt (NTMB) was accompanied by magmatism that formed the Northern Taiwan Volcanic Zone (NTVZ; 2·8–0·2 Ma). The geochemical characteristics of the NTVZ magmas can thus provide constraints both for the mantle source composition and the geodynamic processes operating in the late orogenic stage of the region. The NTVZ volcanic rocks consist dominantly of calc-alkaline andesites and basalts, along with subordinate but heterogeneous lavas including low-K, shoshonitic and ultrapotassic magmas. From the NE to the SW in the NTVZ, the magmas show systematic compositional variations from low-K to calc-alkaline and then shoshonitic. This spatial geochemical variation, characterized by southwesterly increase in potassium and incompatible trace elements, appears to be subparallel to the southwestern part of the modern Ryukyu subduction system. Sr–Nd isotope ratios of the NTVZ volcanic rocks ($^{87}Sr/^{86}Sr \approx 0{\cdot}70376–0{\cdot}70551$; $^{143}Nd/^{144}Nd \approx 0{\cdot}51259–0{\cdot}51301$) suggest that two mantle source components are involved in the magma generation, the asthenosphere and metasomatized subcontinental lithospheric mantle. These two components are represented by the 2·6 Ma Mienhuayu high-Mg basaltic andesites and the 0·2 Ma Tsaolingshan high-Mg potassic lavas, respectively. The latter are interpreted to be the products of small-degree melting of a phlogopite-bearing, harzburgite lithospheric mantle source metasomatized recently by the nearby Ryukyu subduction zone processes. The Sr–Nd–Pb isotope systematics and specific trace-element ratios of the NTVZ volcanic rocks suggest that melts derived from subducted sediments and fluids released from slab dehydration reactions were both involved in metasomatizing this mantle source. The unique spatial geochemical variation of the NTVZ volcanic rocks can be successfully modelled using variable degrees of partial melting of the mantle source regions, coupled with mixing of different melt components from depleted asthenospheric and metasomatized lithospheric mantle components beneath individual volcanic fields. It is inferred that mixing of melts from specific mantle components and the degree of partial melting are spatially and temporally related to the tectonic evolution of the northern Taiwan region, and not simply due directly to subduction zone processes. The overall NTVZ geochemical characteristics can be explained by various degrees of melting within an ascending region of the asthenospheric mantle, triggered by extensional collapse of the NTMB, and interaction of these melts with overlying fluid- and sediment-modified lithospheric mantle.

*Corresponding author. Present address: GEMOC, Department of Earth and Planetary Sciences, Macquarie University, Sydney, N.S.W. 2109, Australia. Fax: 61-2-9850 8943. E-mail: kwang@els.mq.edu.au

Journal of Petrology 45(5) © Oxford University Press 2004; all rights reserved

KEY WORDS: *Northern Taiwan Volcanic Zone; post-collisional magmatism; Pb isotopes; subduction components; geodynamics of basalt genesis*

INTRODUCTION

The tectonic evolution of orogenic belts is typically marked by changes in the composition of the associated magmatism (e.g. Harris *et al.*, 1986). Post-collisional magmatism is one of the common features of many orogens around the world, and may indicate that the orogen is in the process of collapsing (Dewey, 1988). Petrogenetic studies of post-collisional magmatism not only provide constraints on the geodynamic processes responsible for the cessation of collision and onset of extensional collapse, but also reveal changes in magma source regions associated with such processes. In addition, one of the prevailing characteristics of post-collisional magmatism is its subduction-related geochemical characteristics despite subduction processes having been terminated as a result of continental collision. The subduction-related signatures are attributed to metasomatism by slab-derived fluids of the mantle lithosphere prior to collision (Pearce *et al.*, 1990; Turner *et al.*, 1992, 1993, 1996; Platt & England, 1993). Thus, the geochemical characteristics of calc-alkaline post-collisional magmatism allow the evaluation of subduction-related metasomatism of their mantle source.

Taiwan is an active mountain belt created by the oblique collision between the northern Luzon arc and the Asian continent (see Teng, 1990). Despite continuing plate convergence in central and southern Taiwan, extensional collapse has occurred in the northern part of the mountain belt since Plio-Pleistocene times. Accordingly, Teng (1996) proposed a model for the orogenic evolution of northern Taiwan, from mountain building induced by collision to subsequent extensional collapse, lasting only a few million years. Wang *et al.* (1999) proposed that post-collisional extension in the northern Taiwan mountain belt (NTMB) caused the magmatism of the Northern Taiwan Volcanic Zone (NTVZ) (Fig. 1). Compared with other collision orogens also characterized by extensional collapse (Dewey, 1988; Platt & Visser, 1989; Malavielle, 1993), northern Taiwan may provide one of the most active examples of such a tectonic process. In this study, we aim to: (1) investigate the petrogenesis of the post-collisional magmatism, which displays distinctive spatial and temporal geochemical variations indicative of changes in magma source region; (2) explore metasomatism of the mantle source by different subduction components, e.g. hydrous fluids and subducted sediments; (3) track the evolution of the mantle source region during the late orogenic stage; (4) show how the geochemical trends within individual magmatic episodes can constrain the nature of geodynamic processes.

REGIONAL GEOLOGY: THE NTVZ

Located at the Asian continental margin at the boundary of the Philippine Sea plate, the island of Taiwan is not only a collision zone but also a transform region between the opposing Luzon and Ryukyu subduction systems (Fig. 1). The Ryukyu subduction and the resultant Ryukyu arc–trench system, active since the Paleogene, are associated with the development of a back-arc basin, the Okinawa Trough, which has a distinct topography (>2000 m below sea level; Fig. 1) and a strong curvature. Driven by the NW movement of the Philippine Sea plate, the northern segment of the Luzon arc is generally believed to have collided with the Asian continental margin at 10 Ma (Teng, 1990). The Taiwan mountain belt, composed of deformed strata of both the Asian continent and the Luzon arc, reaches a maximum altitude near 4000 m in its central part (Fig. 1). Whereas collisional tectonism is still continuing, as evidenced by the prominent crustal shortening in central and southern Taiwan (e.g. Angelier *et al.*, 1986; Yu & Chen, 1994), structural and seismological data demonstrate that the northern part of the Taiwan mountain belt has been subjected to extensional deformation in the Quaternary (Suppe, 1984; Lee & Wang, 1988; Yeh *et al.*, 1991). Thus, Teng (1996) proposed that extensional collapse of the NTMB took place in Plio-Pleistocene times. Consequently, the topographic elevation of the orogen reduces from near 4000 m in central Taiwan to rolling hills in the northeastern part and eventually becomes submerged in the offshore area farther to the NE (Fig. 1).

The NTVZ comprises two major onshore volcanic fields, the Tatun and Keelung Volcano Groups (TTVG and KLVG), and several offshore volcanoes (Fig. 1). The NTVZ volcanic rocks consist dominantly of andesites with calc-alkaline geochemical characteristics, similar to those commonly observed in convergent-margin lavas (e.g. Gill, 1981). Thus, they have conventionally been regarded as the westernmost part of the Ryukyu volcanic arc (Chen, 1990; Juang, 1993; Chung *et al.*, 1995*b*; Teng, 1996). The conventional view was first questioned by Chen (1997), who suggested an extensional rather than a subduction-related tectonic regime for magma generation. To accommodate available geophysical and geological evidence, Wang *et al.* (1999) proposed that the NTVZ resulted from post-collisional extension related to the late Pliocene orogenic collapse of the NTMB. This extension may also account for the reactivation of the opening of the Okinawa Trough that commenced in the middle Miocene (Sibuet *et al.*, 1995) but became inactive after the arc–continent collision in Taiwan. Reactivated rifting in the Okinawa Trough started propagating to the SW from $\sim$1·5 Ma, with accompanying development of the westernmost part of the Ryukyu subduction system towards Taiwan (Chung *et al.*, 2000).

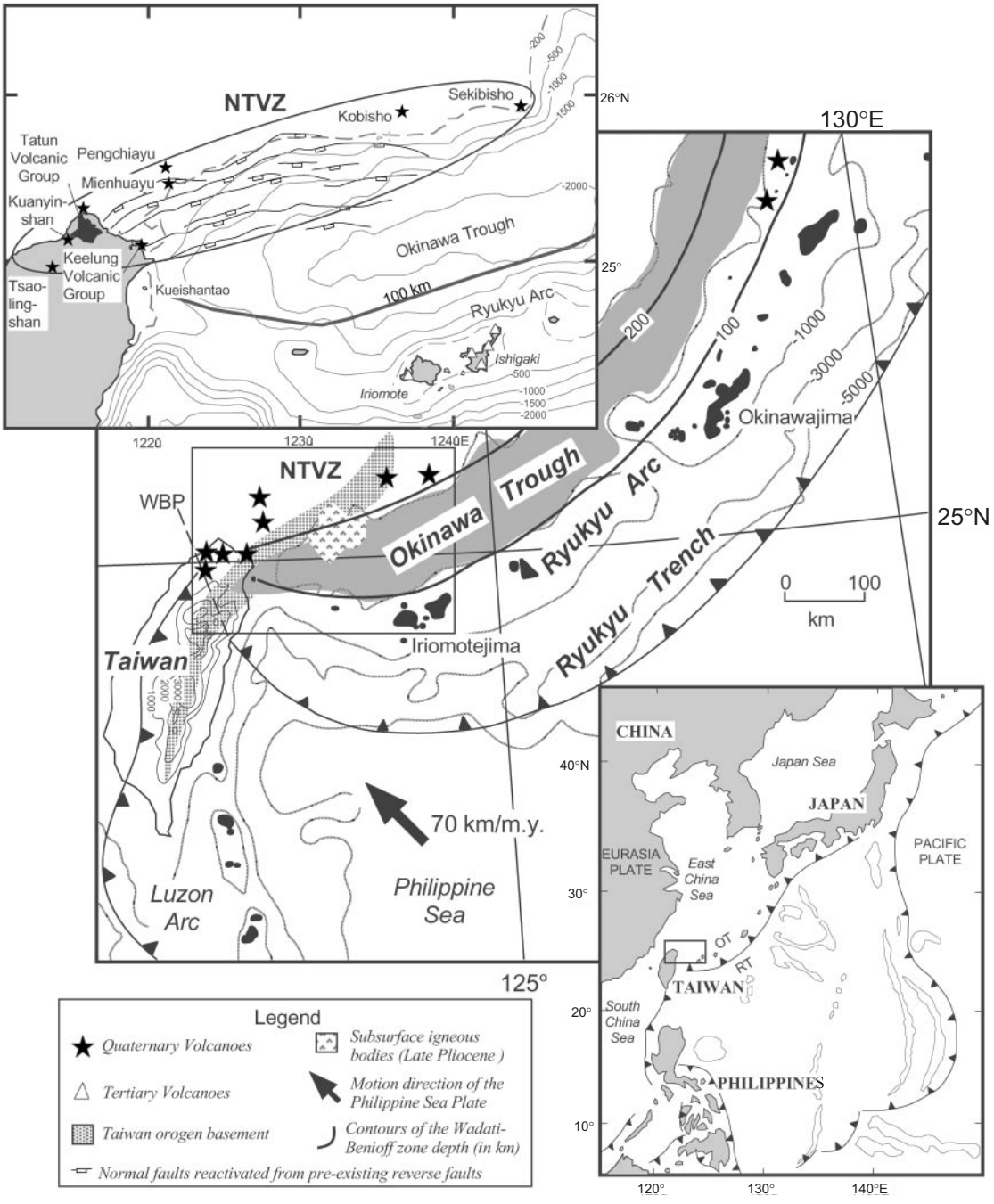

Fig. 1. Maps showing the regional tectonic setting of Taiwan and the volcanic fields of the NTVZ, modified from Wang *et al.* (1999, 2002). WBP indicates the western boundary of the subducting Philippine plate. It should be noted that the NTVZ is currently located ~200 km above the Wadati–Benioff zone. Stippled area represents the Taiwan orogen basement characterized by folded and tilted Tertiary strata (Wageman *et al.*, 1970; also named southern Taiwan–Sinzi Folded Zone). Lower right inset: tectonic setting of Taiwan. OT, Okinawa Trough; RT, Ryukyu Trench. Upper left inset: detailed bathymetric map showing the location of the NTVZ. Bold black line indicates the surface projection of the 100 km contour of the depth to the Wadati–Benioff zone (Sibuet *et al.*, 1998).

Radiometric age data show that the NTVZ volcanism commenced at ~2·8–2·6 Ma and lasted throughout the Quaternary. Figure 2 summarizes existing age data for the NTVZ volcanic rocks, carried out by various dating methods including fission track, K–Ar and Ar–Ar. The age data suggest that the earliest eruptions occurred in the Sekibisho (SBS) and Mienhuayu (MHY) islets and the TTVG around 2·8–2·6 Ma, with the youngest ages

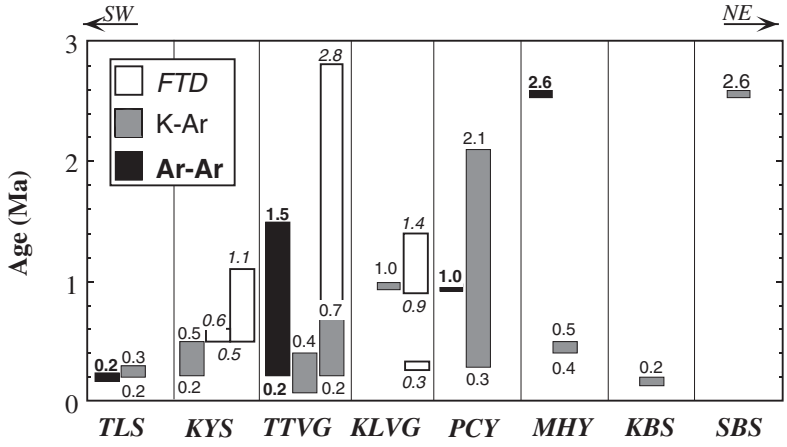

Fig. 2. Radiometric age data for each volcanic field in the NTVZ. Data sources include: fission-track dating (FTD) from Liu *et al.* (1986), Liu (1987) and Wang & Chen (1990); K–Ar ages from Juang (1988, 1993), Shinjo *et al.* (1991) and Tsao (1994); Ar–Ar ages from Lee (1996), Wang *et al.* (2000) and Chung *et al.* (2001*b*). It should be noted that eruption ages of the NTVZ display random distribution relative to their geographical locations. Abbreviations of individual volcanic fields: TLS, Tsaolingshan; KYS, Kuanyinshan; TTVG, Tatun Volcanic Group; KLVG, Keelung Volcanic Group; PCY, Pengchiayu; MHY, Mienhuayu; SBS, Sekibisho; KBS, Kobisho.

around 0·2 Ma in most of volcanic fields. In some localities, however, the volcanic ages might be younger than 0·2 Ma, as dating results are close to or even smaller than the limit of the dating methods. The age spectrum in Figure 2 shows a generally random distribution in space and time, distinct from the southwesterly younging trend of the NTVZ volcanism argued by some workers (e.g. Teng *et al.*, 1992; Teng, 1996). This trend, based on limited geochronological data, was ascribed to southwesterly propagation of the Ryukyu subduction system (Teng *et al.*, 1992). However, when more recent age data (Juang, 1993; Tsao, 1994; Lee, 1996; Wang *et al.*, 2000; Chung *et al.*, 2001*b*) are included, the alleged trend disappears (Fig. 2) so that the argument by Teng *et al.* (1992) and Teng (1996) is problematic.

SAMPLES AND ANALYTICAL METHODS

Samples and major-, trace-element and Nd–Sr isotope methods

Representative volcanic samples were collected from different localities in the NTVZ for detailed geochemical investigation, including whole-rock major- and trace-element, and Sr–Nd–Pb isotope determinations. Geochemical data for the SBS and Kobisho (KBS) volcanic rocks from Shinjo (1998, and unpublished Pb data, 2003) and some Nd–Sr isotope data from Chen (1989) are also included in this paper for comparison. All NTVZ volcanic rocks are microscopically porphyritic. Lithology and phenocryst assemblages are (1) plagioclase + olivine ± titanomagnetite for SBS basalts; (2) plagioclase + olivine + augite for KBS basalts; (3) olivine + bronzite + plagioclase for MHY basaltic andesites; (4) plagioclase + olivine + bronzite for Pengchiayu (PCY) basalts; (5) plagioclase + augite + hornblende + biotite for KLVG dacites; (6) plagioclase + augite + olivine for TTVG basalts and plagioclase + augite + hypersthene + hornblende for andesites; (7) olivine + augite + plagioclase for Kuanyinshan (KYS) basalts and plagioclase + augite + hypersthene + hornblende ± olivine for andesites; (8) olivine + diopside + phlogopite + Fe–Ti oxide ± leucite for TLS absarokites. Detailed petrographic descriptions and mineral chemical data have been reported in a number of publications (Chen, 1990; Juang, 1993; Shinjo, 1998; Wang *et al.*, 2000, 2002; Chung *et al.*, 2001*b*), and so in this paper we focus only on the whole-rock geochemistry of the NTVZ volcanic rocks.

Powder samples were prepared using a jaw crusher and a corundum mill. Major-element compositions were determined by X-ray fluorescence (XRF) using a Rigaku® RIX 2000 spectrometer at the Department of Geosciences, National Taiwan University. The analytical uncertainties are generally better than 5% for all elements (Lee *et al.*, 1997). Loss on ignition was determined by routine procedures. Powdered samples weighing about 50 mg were dissolved using a HF–HNO_3 (10:1) mixture in screw-top Teflon Savillex® for 7 days at ~100°C, followed by evaporation to dryness, refluxing in 7N HNO_3 and drying again, and then dissolving the sample cake in 2% HNO_3. An internal standard solution of 10 ppb Re was added and the spiked dissolutions were diluted with 2% HNO_3 to a sample/solution weight ratio of 1/1000. The internal standard was used for monitoring the signal shift during inductively coupled plasma-mass spectrometry (ICP-MS) measurements using a Perkin Elmer® Elan-6000 spectrometer at Guangzhou

Institute of Geochemistry, the Chinese Academy of Sciences, China, which has a good stability range within ~10% variation (Liu *et al.*, 1996; Li, 1997). Values recommended for the USGS rock standard BCR-1 (Govindaraju, 1994) were used for data calibrations; the analytical errors are generally better than 5% for most trace elements. The samples were dissolved for Sr and Nd separation using routine cation-exchange column techniques. Sr and Nd isotope ratios were measured using VG354® and Finnigan MAT 262® mass spectrometers, respectively, at the Institute of Earth Sciences, Academia Sinica, Taiwan. Detailed chemical and mass spectrometric procedures were described by Chen *et al.* (1990). The isotopic ratios were corrected for mass fractionation by normalizing to $^{86}Sr/^{88}Sr = 0{\cdot}1194$ and $^{146}Nd/^{144}Nd = 0{\cdot}7219$. Long-term laboratory measurements for SRM 987 Sr and La Jolla (UCSD) Nd standards yield $0{\cdot}71024 \pm 0{\cdot}00004$ (2σ) and $0{\cdot}51187 \pm 0{\cdot}00003$ (2σ), respectively. During the period of the study, measurements for the NIST standard SRM 987 gave $^{86}Sr/^{88}Sr = 0{\cdot}71023 \pm 0{\cdot}00001$ (2σ; $n = 3$), and for the La Jolla (UCSD) Nd standards gave $0{\cdot}511867 \pm 0{\cdot}000006$ (2σ; $n = 3$). The overall blank contributions were 0·8 ng Sr for about 20 μg Sr and 0·3 ng Nd for about 0·6 μg Nd in the samples.

Double-spike Pb method

Chemical separation of Pb for isotope analysis was undertaken at the National Taiwan University, Taiwan and the University of the Ryukyus, Japan. Rock chips and/or powders were leached with 6N HCl at ~80°C for 30 min. Then they were rinsed with distilled water before being decomposed with HF and HNO_3. The Pb was separated using standard HBr anion exchange procedures in Teflon columns and the sample solution passed through the columns twice for purification. All chemical processes resulted in loss of about 50% of the Pb in chip samples and 90% in powders, respectively. Two small aliquots of the purified Pb sample were loaded onto two single Re filaments used for natural and double-spiked sample runs separately. A small drop of ^{207}Pb–^{204}Pb double-spike solution and Pb emitter silica gel–H_3PO_4 solution, prepared according to Gerstenberger & Haase (1997), were then added to the aliquot on the mix run filament. Repeated sucking back and release of the mixture with the loading pipette ensured a good sample–spike mixture. Lead isotope measurements were made on a Finnigan MAT262® mass spectrometer using static multi-collector mode at the University of the Ryukyus, Japan. Data acquisition was usually performed at a filament temperature of about 1050–1150°C and consisted of four blocks of data per run, with each block comprising ten 16 s integrations (thus, 160 s integration time per block). Lead isotope ratios were corrected for mass fractionation by the use of a ^{207}Pb–^{204}Pb double-spike method. A new ^{207}Pb–^{204}Pb double-spike solution was prepared and calibrated in this study. The spike calibration is briefly described as follows.

The isotope composition of the newly prepared ^{207}Pb–^{204}Pb double spike was calibrated with NIST Pb standard SRM 982. The standard had been measured in separate natural and mix runs with the new double spike for calibrating the isotopic compositions of the double spike. The isotopic compositions of SRM 982 in the natural runs ($n = 22$ in the period of analysis) were normalized to $^{208}Pb/^{206}Pb = 1{\cdot}00016$, a value recommended by Cameron *et al.* (1969) and accepted in other Pb double-spike and triple-spike studies (e.g. Galer & Abouchami, 1998; Thirlwall, 2000). Data from these SRM 982 analyses and from double-spiked SRM 982 mix runs ($n = 8$) were then used to correct for mass fractionation effect and to determine the isotopic composition of the double spike. All calculations were performed by an iterative technique using an Excel spreadsheet (Woodhead *et al.*, 1995). The $^{204}Pb/^{207}Pb$ was determined to be ~0·9921 in the newly prepared double-spike solution. Once the double-spike composition was calibrated it was tested by obtaining the isotope composition of NIST Pb Standard SRM 981 with the double-spike method. All mixed samples measured ($n = 54$) had $Q \approx 0{\cdot}7$–$0{\cdot}9$ [$Q = {}^{204}Pb_{spike}/({}^{204}Pb_{spike} + {}^{204}Pb_{sample})$]. The double-spike calibrated SRM 981 has the following composition: $^{206}Pb/^{204}Pb = 16{\cdot}9411 \pm 42$, $^{207}Pb/^{204}Pb = 15{\cdot}4978 \pm 52$ and $^{208}Pb/^{204}Pb = 36{\cdot}7185 \pm 142$ (2σ), which agrees well with values recently reported by Galer & Abouchami (1998) and Thirlwall (2000) using triple-spike and double-spike methods, respectively. The external reproducibility of the SRM 981 (2SD, 54 analyses in the period of this study) is 124 ppm for $^{206}Pb/^{204}Pb$, 112 ppm for $^{207}Pb/^{204}Pb$ and 96 ppm for $^{208}Pb/^{204}Pb$. The overall blank contributions were 0·4 ng Pb for about 0·2 μg Pb in the samples. Accordingly, high-quality Pb isotope data were produced for this study using the double-spike method.

The major- and trace-element and Sr–Nd–Pb isotopic compositions of the NTVZ volcanic rocks are presented in Tables 1 and 2, respectively.

WHOLE-ROCK GEOCHEMICAL COMPOSITION

Major-element compositions

In a plot of K_2O vs SiO_2 (Fig. 3a), most of the NTVZ volcanic rocks display calc-alkaline characteristics except for the SBS and MHY magmas, which are low-K, and the TLS magmas, which are shoshonitic. Volcanic rocks from the offshore volcanoes are principally mafic to intermediate, whereas the onshore volcano groups are intermediate to felsic. The mafic rocks ($SiO_2 \leq 55$ wt %) from

Table 1: Whole-rock major- and trace-element compositions for the NTVZ volcanic rocks

Volcanic field:	Sekibisho (SBS)[1]			Kobisho (KBS)					Mienhuayu (MHY)										
Sample no.:	SBS-1	SBS-2	SBS-7	KBS-1[1]	KBS-3[1]	KO-3	KO-4	KO-5	MHH-01	MHY-1	MHY-2	MHY-3	MHY-4	MHY-5	MHY-7	MHY-8	MHY-9	MHY-2-1	MHY-2-2
Major element (wt %)																			
SiO_2	49·91	53·02	50·15	50·66	50·21	49·30	50·02	48·65	54·50	53·30	53·70	53·28	49·44	49·99	53·41	53·56	52·82	53·45	54·21
TiO_2	0·88	0·83	1·02	0·85	0·85	0·76	0·83	0·85	1·44	1·56	1·64	1·50	1·68	1·61	1·53	1·52	1·48	1·54	1·41
Al_2O_3	20·27	17·39	18·84	16·12	16·97	17·20	17·49	17·13	14·60	14·52	15·01	14·35	14·26	14·81	14·35	14·50	14·58	14·49	14·24
Fe_2O_3*	10·60	10·58	11·52	9·52	9·28	9·11	9·13	9·79	10·39	10·79	10·19	10·65	11·46	11·10	10·58	10·55	10·63	10·69	10·34
MnO	0·17	0·22	0·18	0·16	0·16	0·15	0·16	0·16	0·14	0·14	0·13	0·14	0·13	0·13	0·13	0·14	0·13	0·14	0·14
MgO	4·38	5·09	4·73	6·60	6·66	7·08	5·95	6·85	7·38	7·80	5·90	8·08	6·46	6·69	7·82	7·87	7·05	7·48	8·08
CaO	10·44	9·61	10·16	11·42	11·26	12·59	11·81	11·66	8·48	8·22	8·05	8·00	7·28	7·91	8·22	8·03	7·88	8·44	8·27
Na_2O	2·97	2·67	2·88	2·60	2·55	1·82	2·11	1·87	2·14	2·47	2·66	2·72	2·47	2·53	2·67	2·66	2·73	2·45	2·34
K_2O	0·26	0·43	0·36	1·67	1·64	1·48	1·74	1·66	0·40	0·41	0·47	0·42	0·55	0·45	0·43	0·42	0·53	0·42	0·59
P_2O_5	0·10	0·16	0·15	0·39	0·41	0·36	0·42	0·43	0·13	0·54	0·69	0·23	3·41	2·06	0·14	0·14	0·65	0·51	0·29
LOI	1·67	1·11	1·17	1·63	0·99	0·00	0·62	0·38	1·51	0·48	0·93	0·09	1·87	1·60	0·00	0·08	0·54	0·45	0·76
Total	99·98	100·00	99·99	99·99	99·99	99·85	100·28	99·43	101·10	100·22	99·38	99·46	99·02	98·87	99·27	99·47	99·01	100·06	100·67
Mg no.	0·47	0·51	0·47	0·60	0·61	0·63	0·59	0·60	0·61	0·61	0·56	0·62	0·55	0·57	0·62	0·62	0·59	0·60	0·63
Trace element (ppm)																			
Sc	32·8	34·0	30·0	37·3	36·6	24·3	32·6	22·4	21·5	n.d.	n.d.	n.d.	21·8	60·6	67·9	18·8	54·4	21·1	13·5
V	297	276	281	254	251	230	263	279	170	83	89	142	137	149	141	143	141	143	139
Cr	41	28	27	96	93	127	144	92	371	241	188	411	422	424	425	434	429	381	414
Co	29·0	29·0	31·0	36·0	36·0	38·7	35·0	39·7	42·0	24·2	21·0	42·4	37·0	37·2	41·5	45·6	40·6	30·8	31·4
Ni	19·0	13·0	16·0	35·0	35·0	40·2	64·7	35·9	138·2	82·5	51·5	141·3	94·4	102·0	139·8	143·5	154·0	132·8	178·1
Cu	n.d.	n.d.	n.d.	n.d.	n.d.	72·8	83·0	77·3	39·3	18·3	12·7	36·2	38·9	36·7	30·1	36·5	47·3	32·1	54·3
Zn	n.d.	n.d.	n.d.	n.d.	n.d.	65·2	70·0	74·1	110·0	64·8	72·2	102·0	116·5	106·6	103·1	117·0	96·7	135·3	117·0
Ga	n.d.	n.d.	n.d.	n.d.	n.d.	16·4	18·3	17·2	18·7	10·7	11·3	19·1	20·1	20·8	20·0	19·1	19·7	19·1	17·6
Rb	6	9	6	70	67	44	64	46	16	10	12	15	14	15	16	16	19	17	22
Sr	268	265	392	433	436	421	419	492	187	139	110	178	334	222	195	190	216	212	222
Y	20·7	24·5	25·4	19·2	19·5	17·7	18·4	20·2	22·2	12·3	13·6	19·4	13·8	21·9	20·2	19·7	23·4	20·5	18·4
Zr	47·0	54·0	67·0	81·0	82·0	74·4	88·1	89·1	92·0	50·8	56·9	82·9	90·4	90·7	85·0	84·6	83·6	83·5	80·6
Nb	1·9	2·0	2·5	3·7	3·7	3·5	4·2	4·1	6·5	3·5	4·4	5·3	5·8	6·0	5·4	5·3	6·4	5·6	7·9
Cs	0·28	0·44	0·30	1·41	1·34	0·72	1·26	0·66	0·50	0·26	0·27	0·53	0·49	0·48	0·51	0·51	0·64	0·38	0·52
Ba	87	110	137	234	241	215	232	254	137	102	91	131	151	140	139	136	172	94	124
La	3·83	4·77	7·16	7·96	8·23	7·27	7·87	8·63	5·58	3·72	4·22	5·03	4·75	5·23	4·57	4·86	6·18	4·90	7·10
Ce	9·7	11·6	17·5	17·7	18·2	16·6	17·8	19·7	12·4	6·8	7·6	11·3	11·4	12·0	10·6	10·9	13·6	11·0	15·3
Pr	1·46	1·70	2·54	2·35	2·43	2·18	2·41	2·56	1·73	1·13	1·26	1·63	1·63	1·81	1·59	1·64	1·99	1·59	2·15

Volcanic field:	Sekibisho (SBS)[1]			Kobisho (KBS)					Mienhuayu (MHY)										
Sample no.:	SBS-1	SBS-2	SBS-7	KBS-1[1]	KBS-3[1]	KO-3	KO-4	KO-5	MHH-01	MHY-1	MHY-2	MHY-3	MHY-4	MHY-5	MHY-7	MHY-8	MHY-9	MHY-2-1	MHY-2-2
Nd	7·16	8·26	12·03	10·48	10·80	9·88	10·66	11·55	8·85	6·30	7·06	8·25	8·24	9·12	8·05	8·27	9·48	8·36	9·99
Sm	2·24	2·52	3·36	2·81	2·87	2·55	2·85	2·92	3·15	2·10	2·32	3·15	2·96	3·39	3·04	3·09	3·27	2·94	3·05
Eu	0·834	0·912	1·152	0·981	0·998	0·920	1·008	1·020	1·217	0·830	0·880	1·240	1·170	1·380	1·260	1·270	1·300	1·061	1·028
Gd	2·74	3·03	3·79	3·11	3·17	2·99	3·41	3·46	4·07	2·64	2·81	3·57	3·25	3·78	3·41	3·56	3·73	3·45	3·31
Tb	0·494	0·537	0·641	0·507	0·521	0·490	0·545	0·560	0·657	0·440	0·470	0·690	0·640	0·750	0·690	0·690	0·700	0·646	0·593
Dy	3·33	3·63	4·19	3·16	3·26	2·90	3·32	3·25	3·90	2·60	2·86	3·89	3·48	4·26	3·87	3·85	3·98	3·80	3·57
Ho	0·736	0·812	0·912	0·661	0·678	0·620	0·702	0·700	0·752	0·480	0·530	0·780	0·700	0·830	0·780	0·770	0·800	0·663	0·622
Er	2·16	2·42	2·67	1·88	1·93	1·80	2·03	2·08	1·95	1·30	1·45	2·02	1·79	2·18	2·04	2·04	2·10	1·76	1·66
Tm	0·335	0·377	0·413	0·286	0·294	0·260	0·293	0·290	0·285	0·180	0·200	0·280	0·240	0·300	0·280	0·270	0·290	0·243	0·230
Yb	2·15	2·42	2·62	1·80	1·85	1·70	1·87	1·93	1·69	1·11	1·23	1·68	1·42	1·84	1·72	1·71	1·76	1·49	1·40
Lu	0·319	0·367	0·387	0·264	0·270	0·240	0·284	0·280	0·245	0·160	0·170	0·250	0·210	0·270	0·270	0·250	0·260	0·214	0·205
Hf	1·35	1·53	1·86	2·08	2·13	1·73	2·19	1·97	2·61	1·63	1·77	2·21	2·40	2·48	2·36	2·25	2·18	2·56	2·36
Ta	0·150	0·160	0·190	0·300	0·290	0·200	0·228	0·240	0·375	0·210	0·260	0·330	0·360	0·380	0·350	0·330	0·400	0·324	0·446
Pb	2·18	2·77	2·38	3·13	3·19	2·45	3·01	3·74	2·24	1·93	1·21	4·77	6·49	6·47	2·78	2·43	3·12	2·45	5·98
Th	0·57	0·65	0·99	1·69	1·72	1·64	1·80	1·93	1·15	0·86	0·88	1·26	0·80	1·47	1·44	1·21	1·66	0·84	0·93
U	0·20	0·31	0·31	0·53	0·53	0·26	0·53	0·35	0·32	0·21	0·21	0·40	0·68	0·46	0·35	0·33	0·41	0·29	0·31

Volcanic field:	Mienhuayu (MHY)							Pengchiayu (PCY)					Keelung Volcanic Group (KLVG)							
Sample no.:	MHY-2-3	MHY-2-4	MHY-2-5	MHY-2-6	MHY-2-7	MHY-2-8	MHY-2-9	Pen-17	Pen-20	PGU-03	PGU-04	PGU-05	PGU-07	TS-3	GML	CKS5-1	L-2	L-15	L-25	CH-7
Major element (wt %)																				
SiO_2	52·76	52·66	52·32	54·20	54·04	53·37	52·96	49·46	51·18	53·12	50·74	53·54	52·84	54·96	56·24	56·25	56·15	57·62	57·11	58·13
TiO_2	1·50	1·43	1·40	1·45	1·46	1·44	1·51	1·12	1·19	1·12	1·09	1·19	1·09	0·58	0·56	0·57	0·54	0·50	0·55	0·46
Al_2O_3	14·48	14·26	13·89	14·43	14·57	14·35	14·16	17·78	17·24	16·74	16·13	15·40	16·45	17·79	18·20	18·12	17·10	18·13	17·69	17·80
Fe_2O_3*	10·77	10·07	10·26	10·56	10·57	10·69	10·76	10·23	9·49	9·45	9·30	9·87	9·54	6·90	6·11	5·88	6·27	6·00	5·72	6·44
MnO	0·14	0·13	0·14	0·14	0·13	0·14	0·14	0·16	0·15	0·14	0·14	0·14	0·14	0·12	0·11	0·12	0·12	0·12	0·13	0·12
MgO	7·71	7·01	7·67	7·89	7·65	7·81	7·44	5·44	5·45	4·83	5·03	6·47	4·99	4·63	4·62	4·35	4·73	3·75	4·06	3·65
CaO	8·51	8·69	8·91	8·20	8·17	7·92	7·87	10·37	10·33	10·13	10·36	9·19	10·22	8·75	7·84	7·28	8·44	7·83	7·39	7·90
Na_2O	2·29	2·48	2·54	2·52	2·57	2·45	2·31	2·28	2·43	1·86	1·87	1·77	1·82	2·55	2·57	2·71	2·68	2·87	2·68	3·12
K_2O	0·45	0·61	0·49	0·50	0·56	0·56	0·54	1·41	1·46	1·52	1·34	0·95	1·43	1·87	1·60	1·62	1·68	1·65	1·80	1·62
P_2O_5	1·01	0·93	0·88	0·25	0·32	0·48	0·76	0·45	0·39	0·38	0·36	0·28	0·37	0·31	0·21	0·37	0·20	0·27	0·33	0·23
LOI	0·52	1·26	1·27	0·12	0·09	0·31	0·87	n.d.	1·23	n.d.	n.d.	n.d.	n.d.	n.d.	n.d.	3·07	n.d.	n.d.	n.d.	n.d.
Total	100·14	99·53	99·77	100·26	100·13	99·52	99·32	98·70	100·54	99·29	96·37	98·80	98·89	98·44	98·06	100·34	97·90	98·74	97·45	99·48
Mg no.	0·61	0·60	0·62	0·62	0·61	0·61	0·60	0·54	0·56	0·53	0·54	0·59	0·53	0·59	0·62	0·62	0·62	0·58	0·61	0·55

Table 1: continued

Volcanic field:	Mienhuayu (MHY)							Pengchiayu (PCY)					Keelung Volcanic Group (KLVG)							
Sample no.:	MHY-2-3	MHY-2-4	MHY-2-5	MHY-2-6	MHY-2-7	MHY-2-8	MHY-2-9	Pen-17	Pen-20	PGU-03	PGU-04	PGU-05	PGU-07	TS-3	GML	CKS5-1	L-2	L-15	L-25	CH-7
Trace element (ppm)																				
Sc	21·7	20·1	20·1	20·8	21·2	21·5	21·7	35·5	44·0	27·2	27·1	24·3	28·2	46·6	26·9	20·4	29·6	24·3	26·8	24·4
V	142	138	127	139	144	142	145	249	232	234	224	174	231	251	221	210	230	222	185	242
Cr	401	346	365	397	408	421	386	40	42	32	38	n.d.	37	60	128	53	126	32	68	26
Co	31·2	28·9	30·9	31·5	30·6	30·6	30·7	34·2	41·7	29·1	28·8	33·9	29·7	21·3	18·8	16·1	55·4	57·4	16·6	34·0
Ni	174·4	150·9	174·9	179·2	166·0	171·2	168·3	20·0	21·6	15·2	16·9	66·4	17·1	26·6	28·1	17·2	29·9	14·7	22·7	10·9
Cu	39·7	49·8	38·0	38·5	33·8	41·0	32·9	n.d.	n.d.	32·8	17·7	36·4	30·6	n.d.	n.d.	n.d.	n.d.	n.d.	n.d.	n.d.
Zn	186·8	166·9	217·8	127·2	130·8	129·4	152·2	82·7	90·5	82·5	77·3	81·5	78·6	178·3	54·9	48·9	48·9	46·7	49·7	46·7
Ga	19·2	18·2	17·8	18·5	19·0	18·9	19·5	n.d.	n.d.	19·1	18·3	18·1	18·4	n.d.	n.d.	n.d.	n.d.	n.d.	n.d.	n.d.
Rb	16	19	17	18	20	20	18	28	42	46	41	29	42	128	78	58	80	76	89	57
Sr	251	228	339	187	157	209	211	540	524	530	510	342	517	391	296	412	321	399	404	403
Y	21·9	23·7	20·8	20·7	19·8	19·4	19·1	21·4	26·6	22·7	21·5	22·1	21·8	22·5	21·4	15·2	17·9	15·9	19·4	12·5
Zr	80·0	78·9	77·6	80·1	82·4	80·9	82·2	93·0	92·2	90·9	85·2	82·4	86·5	110·1	53·1	23·4	53·8	37·0	50·9	42·3
Nb	6·4	6·2	6·0	6·3	7·0	6·9	6·5	6·2	6·3	6·4	6·0	4·7	6·0	7·4	6·6	10·1	6·8	7·6	9·0	3·9
Cs	0·37	0·43	0·39	0·43	0·49	0·46	0·41	0·55	0·92	1·03	0·98	0·68	0·88	7·60	4·91	6·36	5·55	7·67	8·85	3·40
Ba	112	110	107	116	124	116	110	444	371	355	342	232	340	564	475	564	444	513	631	387
La	6·32	7·26	5·66	6·08	6·26	6·16	5·42	9·22	10·97	10·25	9·68	7·68	9·71	16·58	17·61	18·87	14·65	16·45	20·90	9·97
Ce	13·7	14·5	12·1	13·4	13·3	13·2	11·9	21·1	22·3	23·0	21·9	17·4	21·8	29·9	28·0	36·9	27·0	31·4	37·4	19·7
Pr	2·01	2·13	1·79	1·93	1·89	1·87	1·75	2·90	3·25	3·19	3·00	2·45	3·00	3·92	3·99	4·17	3·32	3·56	4·55	2·33
Nd	9·70	10·44	8·76	9·41	9·06	9·11	8·56	13·46	15·15	14·85	14·05	11·79	14·16	15·54	15·51	15·54	12·90	13·42	17·01	9·22
Sm	3·11	3·39	2·91	3·10	2·92	2·93	2·87	3·75	4·11	4·15	3·93	3·68	3·98	3·19	3·09	2·92	2·80	2·77	3·45	2·10
Eu	1·124	1·176	1·044	1·083	1·035	1·062	1·009	1·270	1·401	1·510	1·470	1·380	1·440	0·854	0·870	0·812	0·836	0·772	0·993	0·672
Gd	3·63	3·89	3·33	3·54	3·37	3·31	3·27	3·99	4·53	4·32	4·10	4·09	4·10	3·13	3·21	2·76	2·65	2·47	3·03	2·01
Tb	0·670	0·709	0·639	0·661	0·626	0·612	0·613	0·652	0·744	0·750	0·710	0·730	0·710	0·517	0·486	0·421	0·482	0·442	0·547	0·352
Dy	3·94	4·21	3·73	3·95	3·76	3·63	3·65	3·87	4·43	4·34	4·13	4·35	4·16	3·26	2·97	2·51	2·62	2·36	2·92	1·87
Ho	0·707	0·739	0·654	0·689	0·658	0·637	0·640	0·786	0·902	0·870	0·830	0·860	0·830	0·707	0·636	0·520	0·638	0·570	0·714	0·455
Er	1·87	1·93	1·70	1·79	1·72	1·68	1·69	2·14	2·45	2·33	2·19	2·26	2·23	2·10	1·85	1·52	1·65	1·49	1·88	1·17
Tm	0·259	0·262	0·228	0·241	0·233	0·230	0·233	0·296	0·335	0·340	0·320	0·330	0·330	0·342	0·295	0·244	0·288	0·260	0·340	0·204
Yb	1·56	1·62	1·46	1·54	1·47	1·43	1·43	1·88	2·09	2·07	1·97	1·99	2·00	2·21	1·88	1·59	1·74	1·58	2·12	1·25
Lu	0·224	0·234	0·213	0·217	0·210	0·209	0·211	0·279	0·319	0·300	0·280	0·280	0·290	0·351	0·301	0·247	0·276	0·253	0·347	0·199
Hf	2·50	2·41	2·37	2·46	2·52	2·52	2·52	2·48	2·50	2·67	2·51	2·55	2·53	3·08	1·56	0·90	1·53	1·14	1·48	1·21

JOURNAL OF PETROLOGY VOLUME 45 NUMBER 5 MAY 2004

Volcanic field:	Mienhuayu (MHY)							Pengchiayu (PCY)					Keelung Volcanic Group (KLVG)							
Sample no.:	MHY-2-3	MHY-2-4	MHY-2-5	MHY-2-6	MHY-2-7	MHY-2-8	MHY-2-9	Pen-17	Pen-20	PGU-03	PGU-04	PGU-05	PGU-07	TS-3	GML	CKS5-1	L-2	L-15	L-25	CH-7
Ta	0·376	0·359	0·346	0·365	0·399	0·387	0·375	0·366	0·473	0·380	0·360	0·290	0·360	0·645	0·419	0·612	0·641	0·619	0·542	0·394
Pb	1·86	1·70	0·76	1·65	1·61	6·72	1·17	4·93	5·61	3·23	3·31	2·06	4·89	45·16	7·72	12·86	7·44	10·21	12·55	6·28
Th	0·98	0·91	0·87	0·94	1·09	1·02	0·95	1·64	1·74	1·75	1·66	1·42	1·67	7·10	5·42	6·04	6·90	8·06	8·93	4·06
U	0·27	0·31	0·33	0·29	0·27	0·26	0·26	0·50	0·50	0·54	0·52	0·42	0·53	2·82	2·05	2·15	2·56	2·65	3·09	1·42

Volcanic field:	KLVG	Tatun Volcanic Group (TTVG)							Kuanyinshan (KYS)						Tsaolingshan (TLS)				
Sample no.:	CH-14	A-3	A-4	A-10	A-18	A-31	A-99	A-129	H-B-1	B-2	K-41	K-57	K-60	K-64	K-99	K-108	TLS-1	TLS-3	TLS-8	TLS-12
Major element (wt %)																				
SiO_2	57·07	58·22	55·20	56·01	54·95	56·65	52·61	49·27	51·94	50·10	51·43	51·26	54·52	50·42	59·98	64·20	48·29	47·65	48·36	47·64
TiO_2	0·49	0·54	0·60	0·52	0·75	0·54	0·81	1·54	1·33	1·54	0·85	1·12	0·79	1·07	0·49	0·35	0·81	0·80	0·81	0·82
Al_2O_3	17·73	18·52	19·68	18·01	19·35	17·95	18·86	17·38	17·17	17·26	17·08	15·59	16·98	14·85	18·22	18·89	11·80	12·75	12·20	11·44
Fe_2O_3*	6·69	6·83	7·30	7·12	7·74	7·47	8·05	9·54	9·32	9·38	8·27	8·68	7·23	8·33	4·29	3·28	7·36	7·24	7·25	7·40
MnO	0·13	0·14	0·14	0·14	0·14	0·14	0·14	0·17	0·16	0·16	0·17	0·16	0·15	0·15	0·10	0·09	0·13	0·13	0·13	0·13
MgO	3·90	2·92	3·46	4·42	3·73	3·22	4·55	5·95	6·13	5·80	7·71	7·96	6·67	8·40	3·38	2·22	15·51	14·72	14·83	16·07
CaO	7·72	7·26	8·09	8·27	8·19	6·55	9·15	10·64	10·21	10·42	9·29	10·12	8·91	10·43	6·01	4·71	7·29	7·24	7·27	7·16
Na_2O	3·05	2·94	2·87	2·66	2·79	2·37	2·50	2·23	2·40	2·38	2·72	2·56	2·80	2·17	3·50	4·68	1·80	1·91	1·89	1·74
K_2O	1·65	1·54	1·48	1·76	1·84	1·60	1·70	1·42	1·36	1·53	1·69	1·86	1·72	1·72	2·04	1·91	4·84	4·58	4·82	5·13
P_2O_5	0·24	0·20	0·22	0·26	0·26	0·25	0·20	0·25	0·23	0·25	0·48	0·37	0·47	0·34	0·31	0·27	1·56	1·54	1·55	1·60
LOI	n.d.	1·17	0·63	0·85	1·05	3·68	0·21	0·18	n.d.	n.d.	0·08	n.d.	n.d.	2·41	1·53	n.d.	n.d.	n.d.	0·01	n.d.
Total	98·66	100·28	99·67	100·02	100·43	100·42	98·78	98·57	100·24	98·82	99·75	99·68	100·23	100·29	99·85	100·60	99·39	98·56	99·12	99·13
Mg no.	0·56	0·48	0·51	0·57	0·51	0·48	0·55	0·58	0·59	0·57	0·67	0·67	0·67	0·69	0·63	0·60	0·82	0·82	0·82	0·83
Trace element (ppm)																				
Sc	22·9	14·4	12·3	29·5	29·0	21·7	21·2	24·6	25·2	24·2	34·5	47·4	30·5	48·5	24·0	15·9	28·5	25·6	29·5	25·8
V	238	182	177	273	262	206	281	299	323	319	257	287	219	309	135	59	191	139	190	141
Cr	27	4	3	69	5	14	17	84	112	99	249	282	212	292	63	23	1064	965	958	1145
Co	28·2	17·3	16·5	23·4	23·3	18·1	26·2	35·2	32·8	33·5	34·3	41·3	29·3	42·7	14·3	7·7	47·4	41·9	46·2	44·8
Ni	10·4	6·2	5·8	13·7	8·3	7·0	11·4	30·7	29·7	26·7	105·5	93·2	79·4	93·6	36·2	17·2	492·0	437·4	466·6	511·4
Cu	n.d.	59·8	41·6	n.d.	n.d.	n.d.	134·0	91·6	102·9	102·5	48·8	94·6	40·8	91·7	48·3	18·7	37·0	33·1	38·9	29·8
Zn	55·9	68·2	65·6	60·8	63·5	67·5	79·0	117·1	89·0	87·1	69·0	61·3	65·2	61·2	47·2	39·7	60·0	43·1	57·6	43·0
Ga	n.d.	18·6	18·8	n.d.	n.d.	n.d.	17·8	20·2	19·6	20·4	19·8	17·7	20·0	17·7	21·2	19·2	12·6	12·0	12·8	11·8
Rb	58	44	46	18	84	45	59	45	43	44	99	98	117	85	140	110	1089	2114	1412	1045
Sr	401	412	411	453	431	401	431	463	419	445	771	643	945	630	1394	1382	704	670	733	661
Y	13·5	20·9	18·3	11·8	19·0	14·4	17·8	23·8	22·8	23·3	21·9	22·7	19·6	20·7	15·7	7·6	14·7	12·9	14·8	13·1

Table 1: continued

Volcanic field:	KLVG	Tatun Volcanic Group (TTVG)								Kuanyinshan (KYS)						Tsaolingshan (TLS)				
Sample no.:	CH-14	A-3	A-4	A-10	A-18	A-31	A-99	A-129	H-B-1	B-2	K-41	K-57	K-60	K-64	K-99	K-108	TLS-1	TLS-3	TLS-8	TLS-12
Zr	36·6	67·7	65·6	71·0	69·1	63·6	71·3	108·2	99·0	109·2	120·9	123·5	138·4	113·0	162·9	49·7	118·7	110·8	121·4	111·2
Nb	4·1	5·3	5·1	4·7	5·5	3·6	5·4	9·5	8·3	9·6	14·1	19·4	19·7	17·8	29·4	33·9	16·3	15·4	17·1	15·3
Cs	2·77	1·39	1·45	2·56	2·62	1·89	4·68	4·06	3·53	4·17	3·83	6·62	7·42	1·95	26·10	11·14	136·75	173·89	166·84	125·42
Ba	415	406	402	452	515	396	382	434	420	427	629	558	726	539	1092	1060	938	997	968	1009
La	10·20	16·49	15·31	7·37	15·28	12·78	13·32	19·13	16·78	18·57	28·32	25·59	35·12	22·46	57·66	50·37	24·36	26·16	24·70	25·94
Ce	21·0	32·6	30·5	19·8	31·9	23·3	27·9	41·6	37·2	42·0	54·0	46·8	62·9	43·0	90·8	68·7	48·7	52·0	49·0	52·2
Pr	2·48	4·05	3·64	2·39	4·02	3·35	3·41	5·36	4·75	5·30	6·41	5·67	7·02	5·17	9·37	7·31	5·90	6·25	5·93	6·31
Nd	9·85	16·42	14·88	10·35	16·66	13·81	14·63	23·01	20·68	22·76	24·18	22·24	25·02	20·32	29·47	21·83	23·70	25·63	23·72	25·98
Sm	2·13	3·28	2·96	2·37	3·61	2·76	3·10	4·96	4·45	4·93	4·36	4·43	4·26	4·14	4·01	2·83	4·45	4·88	4·47	4·93
Eu	0·635	0·910	0·860	0·640	0·920	0·818	0·960	1·480	1·330	1·480	1·306	1·365	1·261	1·260	1·117	0·875	1·117	1·144	1·087	1·218
Gd	2·14	3·35	3·03	2·30	3·33	2·47	3·21	4·87	4·52	4·95	3·75	4·07	3·55	3·87	2·70	1·78	3·53	3·60	3·50	3·72
Tb	0·336	0·530	0·470	0·394	0·517	0·380	0·490	0·720	0·690	0·740	0·590	0·627	0·539	0·593	0·433	0·279	0·465	0·510	0·466	0·519
Dy	2·05	3·06	2·69	2·59	3·14	2·32	2·84	3·88	3·77	4·01	3·46	3·71	3·11	3·48	2·38	1·41	2·47	2·62	2·47	2·72
Ho	0·437	0·670	0·600	0·578	0·655	0·503	0·600	0·810	0·790	0·830	0·708	0·745	0·621	0·705	0·485	0·278	0·490	0·532	0·480	0·548
Er	1·30	2·04	1·85	1·71	1·88	1·50	1·83	2·33	2·30	2·41	2·07	2·10	1·84	1·99	1·46	0·77	1·38	1·49	1·37	1·55
Tm	0·211	0·300	0·270	0·256	0·270	0·219	0·250	0·320	0·320	0·320	0·324	0·314	0·289	0·300	0·229	0·104	0·205	0·221	0·204	0·221
Yb	1·39	2·02	1·88	1·69	1·77	1·47	1·79	2·11	2·13	2·18	2·15	2·00	1·89	1·89	1·53	0·70	1·28	1·37	1·29	1·40
Lu	0·224	0·310	0·280	0·266	0·274	0·241	0·260	0·310	0·310	0·310	0·332	0·305	0·300	0·287	0·252	0·103	0·197	0·203	0·196	0·206
Hf	1·15	1·67	1·58	1·95	1·87	1·59	1·75	2·77	2·55	2·85	3·08	3·05	3·52	2·90	4·33	1·47	3·16	3·42	3·17	3·43
Ta	0·363	0·300	0·290	0·264	0·306	0·205	0·280	0·540	0·480	0·550	0·739	1·075	1·055	0·994	1·780	1·986	0·885	0·975	0·925	0·945
Pb	5·83	6·29	7·26	12·02	9·54	8·05	6·88	7·32	7·09	7·15	15·12	13·53	22·30	12·10	40·63	39·03	30·99	27·83	27·10	25·59
Th	3·33	5·60	5·30	2·29	4·86	3·21	6·96	5·92	5·33	5·45	10·48	8·17	14·08	7·91	22·42	23·91	19·17	22·85	19·56	22·88
U	1·12	0·79	0·82	1·85	1·48	1·48	1·15	0·89	0·83	0·86	4·86	3·54	6·35	3·39	10·67	6·26	18·02	21·24	18·42	21·67

Volcanic field:	Tsaolingshan (TLS)																			
Sample no.:	TLS-17	TLS-18	TLS-23	TLS-24	TLS-27	T-16	T-20	T-24	T-30	T-43	T-48	TLS-5	TLS-14	TLS-19	TLS-20	TLS-21	TLS-29	T-17	T-21	T-22
Major element (wt %)																				
SiO_2	47·06	47·02	47·18	47·88	47·03	44·62	47·15	48·83	48·24	48·95	47·93	47·70	47·96	47·58	47·30	47·22	47·29	48·32	47·91	48·54
TiO_2	0·82	0·82	0·83	0·81	0·80	0·80	0·92	0·82	0·83	0·83	0·79	0·80	0·81	0·83	0·83	0·83	0·81	0·84	0·84	0·82
Al_2O_3	12·07	11·98	13·01	11·70	12·86	17·49	12·38	11·71	11·72	11·80	12·04	12·63	12·39	12·20	12·39	12·62	12·52	11·92	12·24	11·56
Fe_2O_3*	7·34	7·38	7·40	7·33	7·35	7·48	8·53	7·71	7·63	7·58	7·50	7·29	7·35	7·38	7·39	7·42	7·58	7·69	7·87	7·77

Volcanic field: Tsaolingshan (TLS)

Sample no.:	TLS-17	TLS-18	TLS-23	TLS-24	TLS-27	T-16	T-20	T-24	T-30	T-43	T-48	TLS-5	TLS-14	TLS-19	TLS-20	TLS-21	TLS-29	T-17	T-21	T-22
MnO	0·13	0·13	0·13	0·13	0·13	0·13	0·14	0·13	0·13	0·13	0·13	0·12	0·13	0·13	0·13	0·13	0·13	0·13	0·13	0·13
MgO	16·01	16·12	14·82	15·16	15·23	13·93	15·52	14·21	14·24	14·25	15·50	15·04	14·91	14·79	14·73	14·76	15·00	14·13	14·39	14·51
CaO	7·08	7·10	7·46	7·27	7·16	7·02	7·48	7·35	7·30	7·26	6·81	7·28	7·33	7·41	7·46	7·49	7·31	7·39	7·45	7·35
Na_2O	1·72	1·72	1·99	1·83	1·77	1·89	1·83	1·89	1·92	1·84	1·73	1·80	2·00	1·86	1·93	1·94	2·15	2·03	1·88	1·95
K_2O	5·10	5·12	4·26	5·28	5·03	3·66	2·84	5·29	5·28	5·49	5·15	4·79	4·34	4·94	4·49	4·31	4·13	4·82	4·44	4·92
P_2O_5	1·57	1·58	1·56	1·57	1·53	1·44	1·66	1·53	1·51	1·59	1·57	1·56	1·56	1·56	1·57	1·57	1·56	1·54	1·54	1·53
LOI	n.d.	n.d.	n.d.	n.d.	0·18	0·58	1·30	0·10	0·80	0·12	0·04	n.d.	n.d.	n.d.	n.d.	n.d.	n.d.	n.d.	n.d.	n.d.
Total	98·90	98·97	98·64	98·96	99·07	99·04	99·75	99·57	99·60	99·84	99·19	99·01	98·78	98·68	98·22	98·29	98·48	98·81	98·69	99·08
Mg no.	0·83	0·83	0·81	0·82	0·82	0·80	0·80	0·80	0·80	0·80	0·82	0·82	0·82	0·81	0·81	0·81	0·81	0·80	0·80	0·80
Trace element (ppm)																				
Sc	25·4	24·0	30·5	28·3	27·7	25·9	29·0	29·3	28·2	28·0	27·0	22·3	22·9	24·0	22·5	23·0	23·3	25·0	25·5	24·9
V	141	192	209	153	189	160	176	143	155	152	148	n.d.	n.d.	n.d.	n.d.	n.d.	n.d.	n.d.	n.d.	n.d.
Cr	1169	1218	979	992	1054	1052	1182	1053	1056	1057	1148	1201	1129	1083	1080	1088	1146	n.d.	n.d.	n.d.
Co	44·5	49·5	48·7	44·7	47·1	45·1	49·6	44·5	44·2	43·4	47·1	126·2	141·7	132·0	134·2	133·7	148·3	n.d.	n.d.	n.d.
Ni	511·7	538·5	487·3	463·6	483·8	463·2	520·5	456·9	449·8	437·3	532·5	405·0	411·0	408·0	409·0	416·0	426·0	n.d.	n.d.	n.d.
Cu	33·9	39·1	45·5	31·8	34·4	32·9	38·5	27·6	34·8	32·4	32·5	n.d.	n.d.	n.d.	n.d.	n.d.	n.d.	n.d.	n.d.	n.d.
Zn	45·3	57·9	60·4	47·7	58·2	47·0	52·5	48·1	52·8	48·7	52·3	n.d.	n.d.	n.d.	n.d.	n.d.	n.d.	n.d.	n.d.	n.d.
Ga	11·9	12·7	14·0	12·0	12·8	14·8	13·9	12·8	12·7	12·8	12·7	n.d.	n.d.	n.d.	n.d.	n.d.	n.d.	n.d.	n.d.	n.d.
Rb	1025	1084	2098	1046	1068	2546	190	1081	1063	1266	1089	n.d.	n.d.	n.d.	n.d.	n.d.	n.d.	n.d.	n.d.	n.d.
Sr	664	720	822	658	703	671	771	648	657	663	662	667	677	697	708	707	673	n.d.	n.d.	n.d.
Y	13·1	14·7	16·1	13·2	14·6	13·7	15·6	14·4	14·3	14·0	13·9	13	17	14	14	16	15	n.d.	n.d.	n.d.
Zr	110·1	116·0	127·4	108·5	117·0	111·1	124·8	111·7	114·8	116·7	114·2	119	119	121	121	121	118	n.d.	n.d.	n.d.
Nb	15·2	16·7	17·9	15·0	16·2	15·1	17·1	14·6	15·4	15·7	15·5	12	12	13	13	13	13	n.d.	n.d.	n.d.
Cs	122·41	122·05	214·44	114·86	123·82	304·55	23·58	120·32	112·95	124·46	118·46	130·79	251·73	135·08	164·77	186·57	183·87	455	386	397
Ba	1022	959	1028	885	922	850	979	851	864	925	920	963	1064	1004	1029	1042	1021	1014	1057	936
La	26·22	24·30	26·04	23·38	23·89	23·14	26·52	24·62	24·30	24·75	24·56	24·02	24·90	25·64	24·65	24·71	25·98	26·1	26·4	25·8
Ce	52·9	48·5	51·8	46·7	47·7	46·8	53·1	49·0	48·2	49·0	49·1	51·4	58·2	58·6	50·9	50·4	49·2	53·7	59·0	51·6
Pr	6·36	5·91	6·33	5·61	5·77	5·66	6·43	5·91	5·82	5·94	5·94	n.d.	n.d.	n.d.	n.d.	n.d.	n.d.	n.d.	n.d.	n.d.
Nd	26·31	23·91	25·40	22·92	23·19	23·21	26·26	24·10	23·83	24·48	24·31	22·16	24·31	23·66	23·16	22·20	22·95	24·1	25·4	25·7
Sm	5·00	4·52	4·79	4·37	4·36	4·40	4·98	4·61	4·57	4·59	4·62	5·90	6·13	6·08	5·68	5·60	5·77	6·1	5·9	6·0
Eu	1·212	1·113	1·183	1·065	1·055	1·134	1·251	1·090	1·149	1·128	1·105	1·046	1·149	1·129	1·117	1·121	1·157	1·3	1·2	1·2
Gd	3·74	3·57	3·76	3·37	3·53	3·37	3·86	3·41	3·35	3·39	3·32	n.d.	n.d.	n.d.	n.d.	n.d.	n.d.	n.d.	n.d.	n.d.
Tb	0·525	0·468	0·497	0·466	0·459	0·480	0·542	0·497	0·491	0·484	0·484	0·924	0·939	1·006	0·879	0·952	0·992	0·98	1·08	0·97
Dy	2·74	2·49	2·68	2·38	2·42	2·47	2·79	2·60	2·57	2·54	2·53	n.d.	n.d.	n.d.	n.d.	n.d.	n.d.	n.d.	n.d.	n.d.
Ho	0·552	0·492	0·524	0·482	0·476	0·499	0·566	0·527	0·522	0·518	0·509	n.d.	n.d.	n.d.	n.d.	n.d.	n.d.	n.d.	n.d.	n.d.

Table 1: continued

Volcanic field:	Tsaolingshan (TLS)																			
Sample no.:	TLS-17	TLS-18	TLS-23	TLS-24	TLS-27	T-16	T-20	T-24	T-30	T-43	T-48	TLS-5	TLS-14	TLS-19	TLS-20	TLS-21	TLS-29	T-17	T-21	T-22
Er	1·55	1·40	1·49	1·37	1·35	1·42	1·62	1·47	1·45	1·43	1·43	n.d.	n.d.	n.d.	n.d.	n.d.	n.d.	n.d.	n.d.	n.d.
Tm	0·227	0·206	0·221	0·198	0·198	0·207	0·235	0·216	0·212	0·207	0·205	n.d.	n.d.	n.d.	n.d.	n.d.	n.d.	n.d.	n.d.	n.d.
Yb	1·41	1·29	1·38	1·21	1·26	1·30	1·44	1·34	1·31	1·28	1·28	1·55	1·65	1·74	1·56	1·03	1·23	1·3	1·3	1·6
Lu	0·212	0·196	0·211	0·185	0·191	0·195	0·214	0·201	0·196	0·192	0·190	0·179	0·208	0·222	0·213	0·217	0·194	0·24	0·21	0·25
Hf	3·46	3·04	3·31	2·95	3·04	3·07	3·41	3·02	3·09	3·13	3·09	2·94	7·21	3·10	3·03	3·09	3·10	3·2	2·8	3·1
Ta	0·959	0·884	0·950	0·832	0·858	0·835	0·937	0·791	0·819	0·844	0·829	0·649	0·751	0·765	0·717	0·745	0·704	0·74	0·84	0·70
Pb	30·02	24·73	32·10	23·45	20·91	19·87	23·29	19·76	19·28	20·15	19·59	25	27	23	24	23	30	n.d.	n.d.	n.d.
Th	23·33	17·68	20·31	19·76	18·75	19·32	21·67	19·76	19·28	20·15	19·59	19·12	19·99	20·53	18·22	18·70	20·54	19·9	20·6	19·6
U	22·13	18·39	19·16	18·21	17·53	18·25	20·01	17·53	17·23	17·58	18·12	21·65	22·42	22·79	21·67	20·94	22·53	20·4	20·4	20·6

Volcanic field:	Tsaolingshan (TLS)					
Sample no.:	T-25	T-33	T-34	T-36	T-41	T-46
Major element (wt %)						
SiO_2	48·37	48·76	47·92	48·16	48·70	48·46
TiO_2	0·83	0·82	0·84	0·81	0·82	0·81
Al_2O_3	12·05	11·49	12·20	11·98	12·37	12·14
Fe_2O_3*	7·63	7·57	7·70	7·46	7·55	7·52
MnO	0·13	0·12	0·13	0·12	0·13	0·13
MgO	14·22	14·19	14·45	14·01	14·40	14·36
CaO	7·25	7·21	7·22	7·14	7·23	7·23
Na_2O	1·91	1·91	1·93	1·91	1·80	1·77
K_2O	5·25	5·37	4·45	5·53	5·08	4·85
P_2O_5	1·52	1·60	1·57	1·57	1·58	1·58
LOI	n.d.	n.d.	n.d.	n.d.	n.d.	n.d.
Total	99·16	99·04	98·41	98·69	99·66	98·85
Mg no.	0·80	0·80	0·80	0·80	0·81	0·81
Trace element (ppm)						
Sc	24·2	24·8	25·5	25·0	24·3	24·6
V	n.d.	n.d.	n.d.	n.d.	n.d.	n.d.
Cr	n.d.	n.d.	n.d.	n.d.	n.d.	n.d.
Co	n.d.	n.d.	n.d.	n.d.	n.d.	n.d.
Ni	n.d.	n.d.	n.d.	n.d.	n.d.	n.d.

JOURNAL OF PETROLOGY | VOLUME 45 | NUMBER 5 | MAY 2004

Volcanic field:	Tsaolingshan (TLS)					
Sample no.:	T-25	T-33	T-34	T-36	T-41	T-46
Cu	n.d.	n.d.	n.d.	n.d.	n.d.	n.d.
Zn	n.d.	n.d.	n.d.	n.d.	n.d.	n.d.
Ga	n.d.	n.d.	n.d.	n.d.	n.d.	n.d.
Rb	n.d.	n.d.	n.d.	n.d.	n.d.	n.d.
Sr	n.d.	n.d.	n.d.	n.d.	n.d.	n.d.
Y	n.d.	n.d.	n.d.	n.d.	n.d.	n.d.
Zr	n.d.	n.d.	n.d.	n.d.	n.d.	n.d.
Nb	n.d.	n.d.	n.d.	n.d.	n.d.	n.d.
Cs	288	282	254	317	283	344
Ba	1053	953	1045	963	927	1027
La	24·6	31·8	26·7	25·9	24·7	26·1
Ce	51·9	56·4	66·8	56·0	55·9	58·0
Pr	n.d.	n.d.	n.d.	n.d.	n.d.	n.d.
Nd	25·7	28·1	27·2	27·0	27·2	24·6
Sm	6·1	6·2	6·6	6·4	6·2	6·4
Eu	1·3	1·2	1·3	1·2	1·2	1·1
Gd	n.d.	n.d.	n.d.	n.d.	n.d.	n.d.
Tb	0·88	1·04	1·09	1·19	1·01	1·05
Dy	n.d.	n.d.	n.d.	n.d.	n.d.	n.d.
Ho	n.d.	n.d.	n.d.	n.d.	n.d.	n.d.
Er	n.d.	n.d.	n.d.	n.d.	n.d.	n.d.
Tm	n.d.	n.d.	n.d.	n.d.	n.d.	n.d.
Yb	1·5	1·8	1·6	1·7	1·6	1·6
Lu	0·21	0·26	0·24	0·24	0·22	0·20
Hf	3·3	3·0	3·2	3·2	2·9	3·3
Ta	0·72	0·74	0·77	0·81	0·76	0·83
Pb	n.d.	n.d.	n.d.	n.d.	n.d.	n.d.
Th	19·6	20·2	21·2	20·4	19·7	20·9
U	20·1	20·2	22·9	21·5	20·6	22·3

Fe_2O_3*, total iron as Fe_2O_3; Mg number = atomic 100 ($Mg/Mg + Fe^{2+}$), assuming $Fe_2O_3/FeO = 0{\cdot}1$; n.d., not determined.
[1]Data from Shinjo (1998).

Table 2: Sr–Nd–Pb isotope compositions for the NTVZ volcanic rocks

Volcanic field	Sample no.	$^{87}Sr/^{86}Sr$	$^{143}Nd/^{144}Nd$	T_{DM}[1]	$^{206}Pb/^{204}Pb$	$^{207}Pb/^{204}Pb$	$^{208}Pb/^{204}Pb$
SBS[2]	SBS-1	0·70406					
	SBS-2	0·70414	0·51289		18·351	15·574	38·524
	SBS-7	0·70376	0·51284		18·283	15·547	38·389
KBS	KBS-1[2]	0·70384	0·51271		18·408	15·580	38·620
	KBS-3[2]	0·70398	0·51271		18·410	15·583	38·627
	KO-4	0·70396	0·51272		18·407	15·587	38·633
	KO-5				18·410	15·586	38·640
MHY	MHH-01	0·70461	0·51298				
	MHY-2	0·70453	0·51301		18·588	15·599	38·729
	MHY-3	0·70446	0·51290				
	MHY-4		0·51294		18·602	15·607	38·767
	MHY-7	0·70438	0·51299		18·577	15·611	38·749
	MHY-8	0·70440	0·51297				
	MHY-9	0·70447	0·51293				
PCY	Pen-20	0·70391	0·51289				
	PGU-04	0·70395	0·51295		18·446	15·574	38·535
	PGU-05	0·70404	0·51297		18·443	15·576	38·531
KLVG	TS-3	0·70482	0·51270	3·74	18·502	15·635	38·830
	GML	0·70489	0·51272	2·66			
	CKS5-1	0·70474	0·51269	1·89			
	L-15	0·70496	0·51270	4·03			
	CH-7	0·70430	0·51282				
TTVG	A-3	0·70469	0·51273	2·63			
	A-10	0·70428	0·51278				
	A-18	0·70456	0·51273				
	A-31	0·70442	0·51268				
	A-129	0·70447	0·51280		18·517	15·627	38·763
	H-B-1	0·70450	0·51276		18·525	15·627	38·763
KYS	K-41	0·70416	0·51284	1·00	18·442	15·618	38·726
	K-64	0·70407	0·51283	2·35	18·439	15·616	38·721
	K-99	0·70427	0·51281	0·55			
	K-108	0·70417	0·51281	0·49			
TLS	TLS-8	0·70546	0·51268	1·97	18·450	15·628	38·775
	TLS-18	0·70551	0·51263	2·21			
	TLS-23	0·70543	0·51266	2·06			
	TLS-27		0·51266	2·05			
	T-16	0·70543	0·51266	2·15	18·450	15·629	38·780
	T-20	0·70542	0·51264	2·25			
	T-24	0·70540	0·51265	2·27			
	T-30	0·70543	0·51268	2·20			
	T-43	0·70546	0·51266	2·00			
	T-48	0·70551	0·51259	2·48			

[1]Nd modal age assuming derivation from a depleted mantle source with $^{143}Nd/^{144}Nd = 0·513114$ and $^{147}Sm/^{144}Nd = 0·222$ (Michard *et al.*, 1985).
[2]Data from Shinjo (1998).
Average analytical 2σ errors: ±0·00004 for $^{87}Sr/^{86}Sr$; ±0·00002 for $^{143}Nd/^{144}Nd$; ±0·004 for $^{206}Pb/^{204}Pb$; ±0·005 for $^{207}Pb/^{204}Pb$; ±0·014 for $^{208}Pb/^{204}Pb$.

the various volcanic fields exhibit a trend of increasing K_2O content and decreasing SiO_2 content from NE to SW (Fig. 3a). In a plot of K_2O vs Na_2O (Fig. 3b), most of the NTVZ volcanic rocks have relatively high K_2O contents, although only the TLS magmas have K_2O contents higher than Na_2O. The high K_2O contents in some onshore volcanic fields with high SiO_2 and Na_2O contents may result from fractional crystallization;

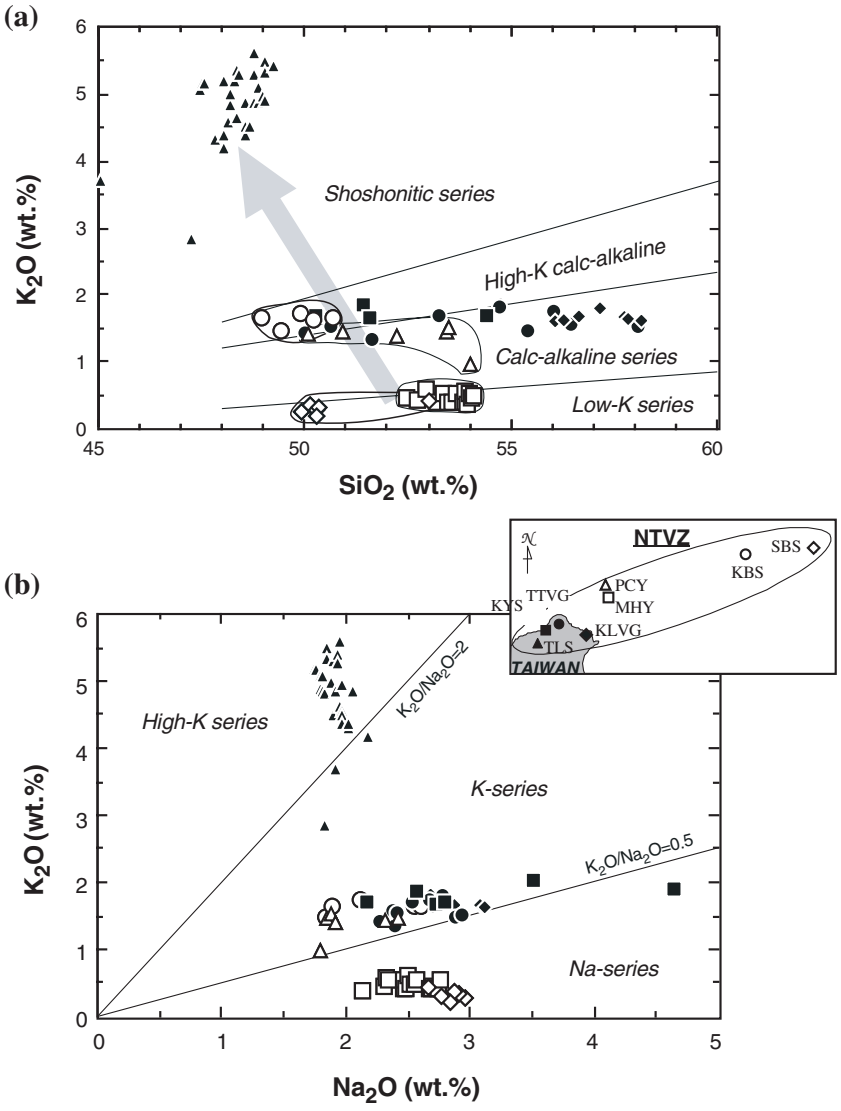

Fig. 3. Variation of K_2O vs SiO_2 (a) and Na_2O (b) for volcanic rocks from the NTVZ. The series boundaries in (a) and (b) are from Gill (1981) and Middlemost (1975), respectively. The grey arrow in (a) indicates the trend of spatial geochemical variation. The inset in (b) is a map showing the distribution of the main volcanic areas and the symbols used in the diagram. (For abbreviations see caption to Fig. 2.)

however, for some of the NTVZ mafic rocks fractional crystallization is not likely to be the reason for the high K_2O contents (Fig. 3). As shown in Harker diagrams of CaO, Fe_2O_3(t), Al_2O_3, Cr, Sr and La vs MgO (Fig. 4), there is no significant trend of fractional crystallization for individual volcanic fields in the NTVZ, except for some onshore volcanic fields (TTVG and KYS).

Some NTVZ volcanic rocks have high Al_2O_3 contents (~17–20 wt %) and may be classified as high-Al basalts (e.g. Chen, 1990). According to the definition of high-Al basalts by Crawford *et al.* (1987) (SiO_2 < 54 wt %; Al_2O_3 >16·5 wt % and MgO < 7 wt %), high-Al basalts occur in most areas of the NTVZ. All volcanic rocks from the SBS are high-Al basalts; however, none was found in the MHY and TLS. The SBS have the lowest Mg number (~0·5) in the NTVZ, whereas the MHY and TLS are relatively primitive magmas (Mg number = 0·6 and 0·8, respectively). The Mg number values for the MHY and TLS basalts are in equilibrium with the Fo contents of their olivine phencrysts (Fo = 81 and 90, resepectively) based on the calculation for olivine–liquid equilibrium (Roeder & Emslie, 1970).

Trace-element compositions

Mafic rocks from the individual volcanic fields in the NTVZ have distinctive trace-element characteristics. The TLS basalts have the highest compatible

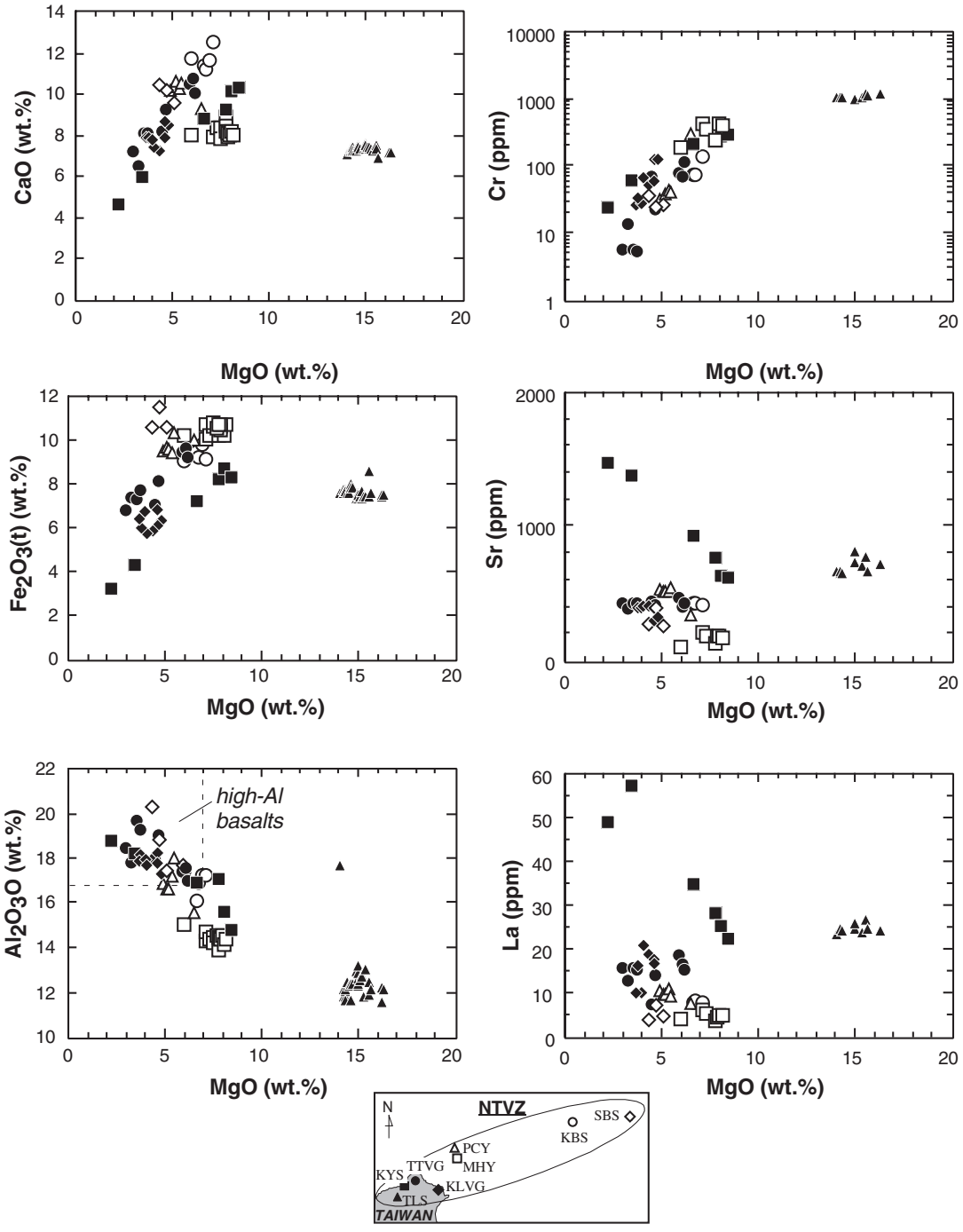

Fig. 4. Variation diagrams of CaO, Fe_2O_3(t), Al_2O_3, Cr, Sr and La vs MgO, respectively, for volcanic rocks from the NTVZ. The inset shows a map of the distribution of the main volcanic areas and the symbols used in the variation diagrams.

trace-element contents (Ni ~500 ppm; Cr ~1000 ppm). This characteristic, together with their major-element chemistry, is consistent with the TLS magmas being near-primary magmas. Incompatible trace-element characteristics are illustrated as chondrite-normalized rare earth element (REE) diagrams in Fig. 5 and as primitive mantle-normalized element diagrams in Fig. 6. The REE patterns of the NTVZ volcanic rocks are light REE (LREE) enriched, but the extent of enrichment is variable between the volcanic fields. The SBS and MHY mafic rocks have the lowest abundances of LREE and show relatively flat REE patterns, whereas the TLS

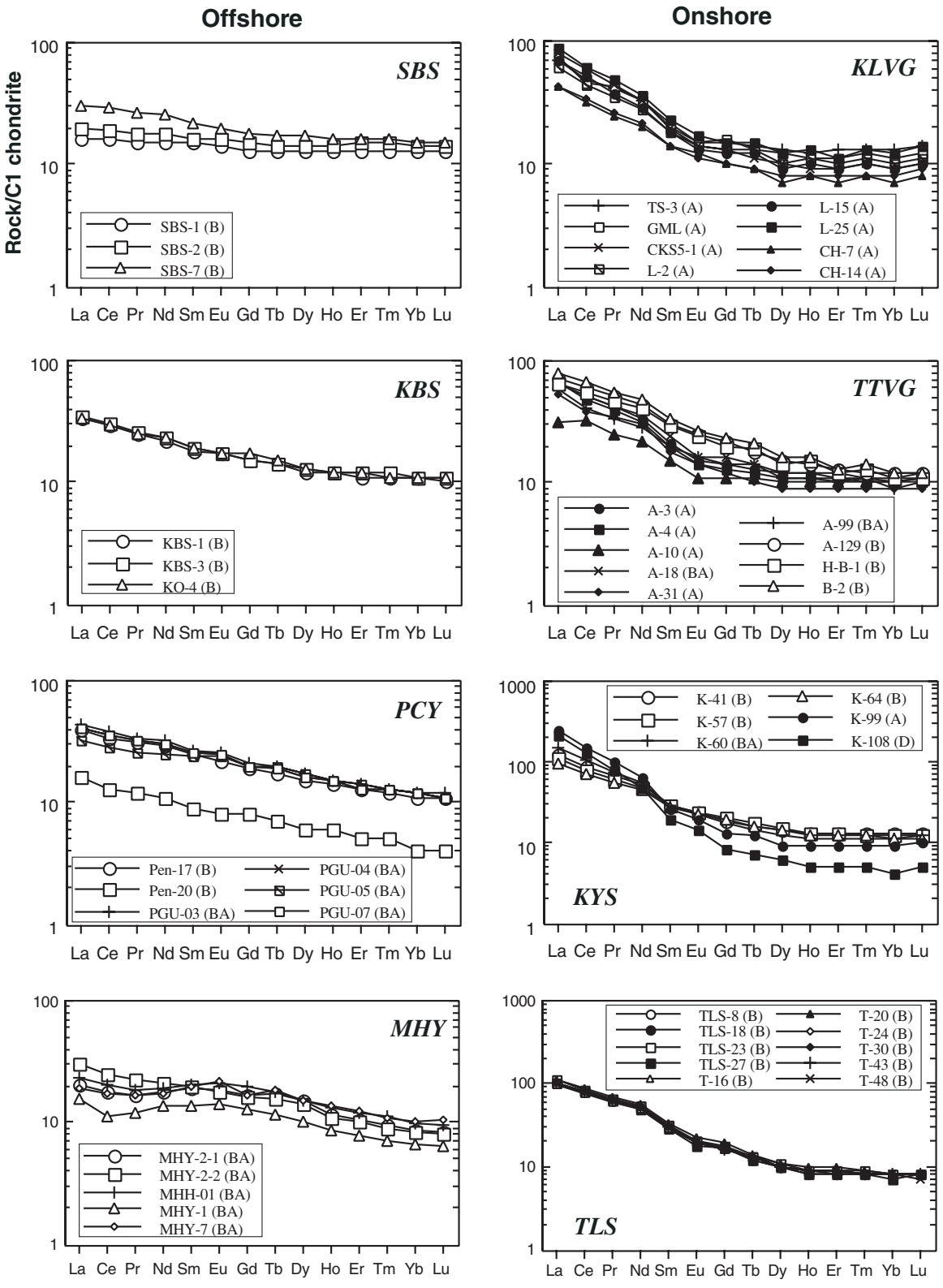

Fig. 5. Chondrite-normalized REE variation diagrams for the NTVZ volcanic rocks. Normalization constants are from Sun & McDonough (1989). The letters in the legend of each diagram represent the lithology: B, basalt; BA, basaltic andesite; A, andesite; D, diorite.

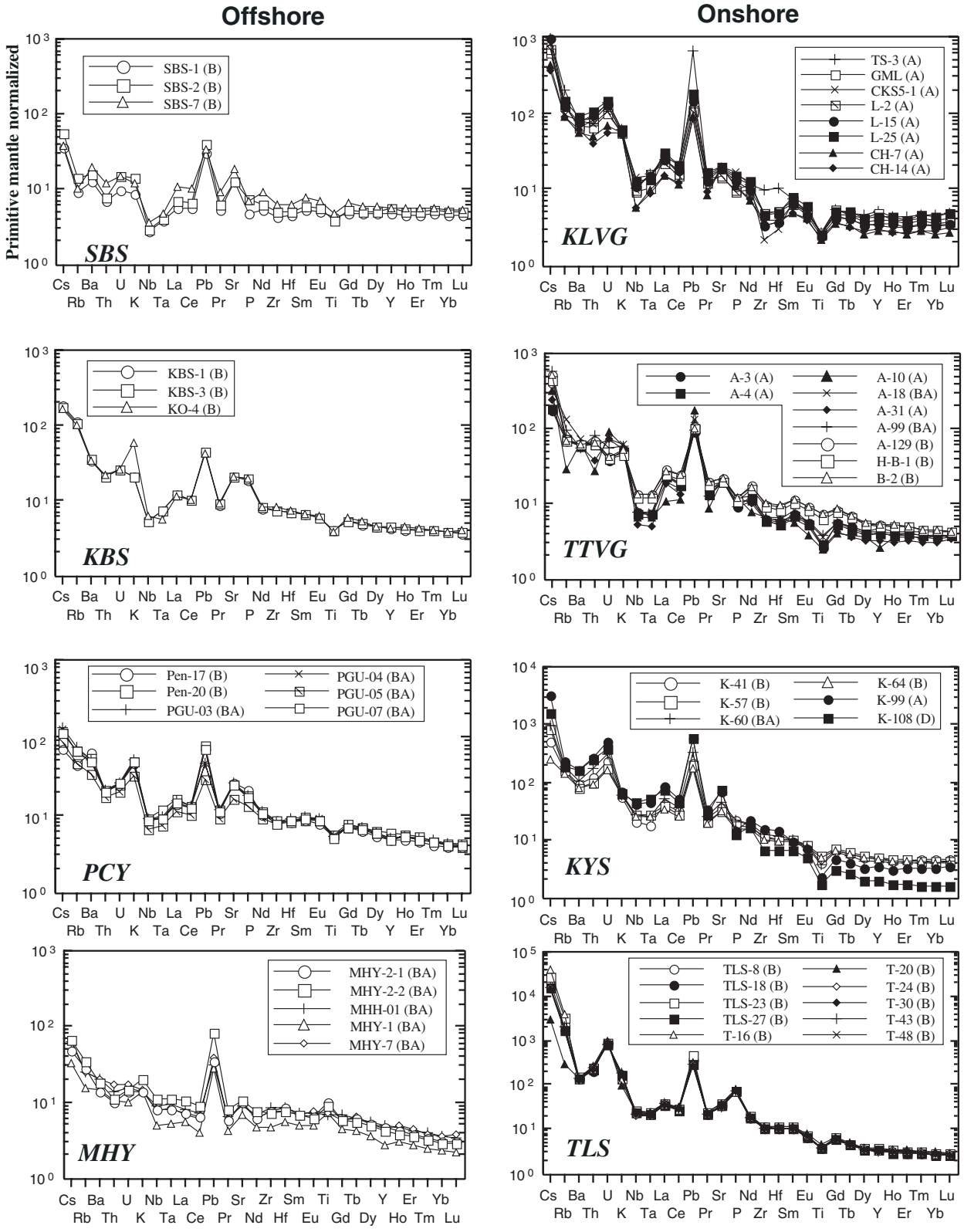

Fig. 6. Primitive mantle-normalized trace-element variation diagrams for the NTVZ volcanic rocks. Normalization constants are from Sun & McDonough (1989).

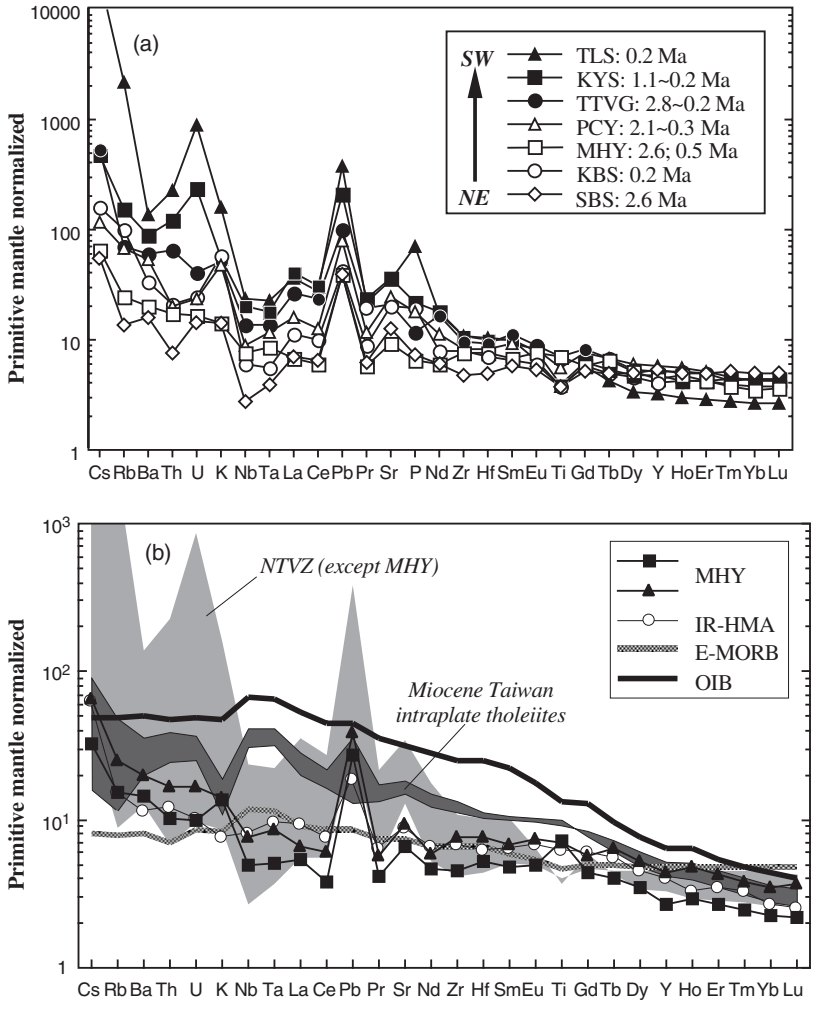

Fig. 7. (a) Primitive mantle-normalized trace-element diagrams for representative volcanic rocks for each volcanic field from the NTVZ. It should be noted that only the mafic members are plotted and therefore KLVG is excluded. (b) Primitive mantle-normalized trace-element variation diagram for representative MHY high-Mg basaltic andesites in comparison with Miocene intraplate basalts from NW Taiwan (MTIB; Chung *et al.*, 1994, 1995*a*), high-Mg andesites of Iriomote-jima, southern Ryukyus (IR-HMA; Shinjo, 1999), E-MORB, ocean-island basalt (OIB) and other NTVZ volcanic rocks. Normalization constants, E-MORB and OIB values are from Sun & McDonough (1989).

basalts are the most LREE enriched. None of the REE patterns has an obvious negative Eu anomaly, which may indicate that plagioclase was not a fractionating phase in the NTVZ volcanic rocks.

The primitive mantle-normalized trace-element patterns of the NTVZ volcanic rocks show significant enrichments in large ion lithophile elements (LILE) and LREE and a pronounced Pb spike (Figs 6 and 7a). Except for the MHY samples, which have relatively smooth trace-element patterns, all the NTVZ volcanic rocks have distinct high field strength element (HFSE; i.e. Nb, Ta and Ti) troughs in their patterns. The TLS magmas have the highest LILE contents, with Rb concentrations up to 2500 ppm, which is the highest reported value for terrestrial rocks (Chung *et al.*, 2001*b*). High LILE and K contents suggest that phlogopite may be present in the mantle source of the TLS magmas (Chung *et al.*, 2001*b*). The most mafic NTVZ volcanic rocks also exhibit systematic enrichment in LILE and LREE from SBS in the NE to TLS in the SW (Fig. 7a), paralleling the spatial variation shown by major-element compositions.

Notably, the MHY magmas do not show HFSE depletion but they show positive Pb spikes in the trace-element plots (Fig. 7b). Overall the trace-element patterns of the MHY magmas are similar to those of Miocene Taiwan intra-plate basalts (MTIB) in northwestern Taiwan (Chung *et al.*, 1994, 1995*a*) although with lower LILE and LREE abundances (Fig. 7b). Additionally, the MHY trace-element patterns are almost the same as those of high-Mg andesites from Iriomote-jima, southern Ryukyu (Shinjo, 1999), considered to be associated with extensional tectonic activity on the Asian

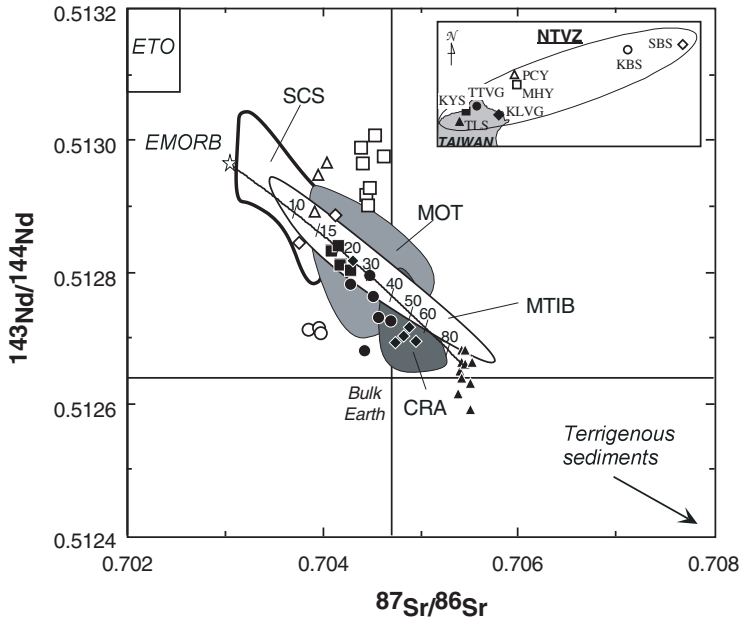

Fig. 8. Variation of $^{87}Sr/^{86}Sr$ vs $^{143}Nd/^{144}Nd$ for the NTVZ volcanic rocks. MTIB from NW Taiwan (Chung *et al.*, 1994, 1995*a*), South China Seamounts (SCS; Tu *et al.*, 1992), back-arc magmas from the middle Okinawa Trough (MOT; Wang, 1998; Shinjo *et al.*, 1999) and basalts from the central Ryukyu Arc (CRA; Shinjo *et al.*, 1999) are also shown as fields for comparison. The East Taiwan Ophiolite (ETO) field is from Jahn (1986) and Chung & Sun (1992). The composition of average terrigenous sediments from Taiwan is from Lan *et al.* (1990). The mixing curve represents variable degrees of mixing between melts derived from MHY and TLS mantle sources. The Sr isotope composition of E-MORB is used to represent the unmodified source of the MHY (the asthenospheric mantle source; see detailed discussion in text). Ticks with a number indicate the percentage involvement of the SCLM (the TLS source).

continental margin in the Miocene (Chung *et al.*, 1994, 1995*a*).

Nd–Sr–Pb isotopic compositions

The TLS samples have the highest Sr isotope ratios ($^{87}Sr/^{86}Sr \approx 0{\cdot}70540$–$0{\cdot}70551$) and lowest Nd isotope ratios ($^{143}Nd/^{144}Nd \approx 0{\cdot}51259$–$0{\cdot}51268$). The MHY samples, however, have the most depleted Nd isotope ratios ($^{143}Nd/^{144}Nd \approx 0{\cdot}51290$–$0{\cdot}51301$) similar to those of enriched mid-ocean ridge basalt (E-MORB; Sun *et al.*, 1979) and the South China Sea (SCS) seamounts (Fig. 8; Tu *et al.*, 1992), but more enriched than that of the Eastern Taiwan Ophiolite (ETO) representing the composition of the local mantle source of depleted MORB (Jahn, 1986; Chung & Sun, 1992). The isotopic composition of the SCS may represent the composition of the local mantle source of E-MORB (Tu *et al.*, 1992). Additionally, the MHY Nd isotope ratios are more depleted than those of typical arc and back-arc magmas in the nearby Central Ryukyu Arc (CRA) and Middle Okinawa Trough (MOT; Fig. 8; Wang, 1998; Shinjo *et al.*, 1999). The MHY and some PCY Sr isotope ratios are slightly elevated so that the data plot to the right of the mantle array in the Nd–Sr isotope diagram (Fig. 8). In terms of the Nd isotope composition, however, the other NTVZ volcanic rocks plot between the depleted MHY and enriched TLS samples. In the Nd–Sr isotope diagram the overall data for the NTVZ show a distribution similar to that of the MTIB magmas, which have been interpreted to have originated by interaction of partial melts of ascending asthenosphere with the overlying sub-continental lithospheric mantle (SCLM) beneath the western Taiwan region (Chung *et al.*, 1994, 1995*a*). The onshore NTVZ volcanic rocks have positive Nd model ages based on a depleted mantle reservoir ($T_{DM} \approx 0{\cdot}5$–$4{\cdot}0$ Ga; Table 2). The TLS magmas are unique in yielding positive ages that fall in a restricted range from 2·0 to 2·5 Ga. Other NTVZ volcanic rocks, which might have been the product of mixing of partial melts of different mantle source components, yield negative Nd model ages (not shown in Table 2).

The NTVZ volcanic rocks have high $^{207}Pb/^{204}Pb$ and $^{208}Pb/^{204}Pb$ at a given $^{206}Pb/^{204}Pb$ ratio (Fig. 9), and all lie above the Northern Hemisphere Reference Line (NHRL) of Hart (1984), consistent with the typical Pb isotopic characteristics of mantle-derived magmas in nearby regions (i.e. ETO, SCS, MOT and MTIB; see Chung *et al.*, 2001*a*, and reference therein). The NTVZ data define a linear trend between the ETO and Ruykyu subducted sediment values (Sun, 1980). However, the NTVZ volcanic rocks show a restricted range in comparison with nearby magmatic provinces, and most of them plot within the SCS field (Fig. 9). Remarkably, unlike the

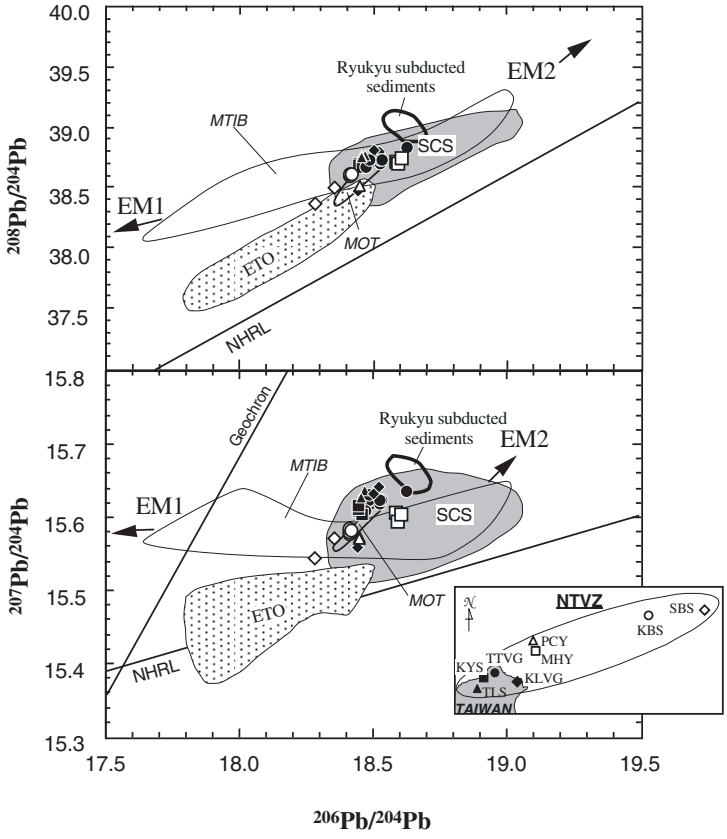

Fig. 9. $^{208}Pb/^{204}Pb$ and $^{207}Pb/^{204}Pb$ vs $^{206}Pb/^{204}Pb$ diagrams for the NTVZ volcanic rocks. Data for the ETO and Ryukyu subducted sediments are from Sun (1980). The enriched mantle components EM1 and EM2 are from Hart (1988). The NHRL is from Hart (1984). Other data sources are the same as in Fig. 8.

major- and trace-element compositions, the Sr–Nd–Pb isotopic compositions of the NTVZ volcanic rocks do not show any systematic NE to SW variation.

DISCUSSION

In the following sections we consider specific aspects of the geochemical characteristics of the NTVZ volcanic rocks including spatial and temporal variations, the mantle source components involved in melt generation, and degrees of partial melting. To minimize the effects of fractional crystallization, the volcanic rocks from the KLVG [which are all intermediate to silicic in composition ($SiO_2 \approx 55$–58 wt %)] are excluded and only mafic rocks ($SiO_2 < 54$ wt %) are considered. Crustal contamination may be an important process in the petrogenesis of the volcanic rocks from the southwestern part of the NTVZ. However, as shown by a plot of $^{87}Sr/^{86}Sr$ vs SiO_2 (Fig. 10a), it does not appear to have a major influence on the isotopic characteristics of the NTVZ volcanic rocks. In Fig. 10a the mixing line between the average composition of the Taiwan upper crust and the MOT basalt (assumed to have a similar mantle source to the NTVZ; see subsequent discussion) defines a steep slope, distinct from the variation trends for the individual volcanic fields in the NTVZ.

Spatial and temporal geochemical variation in magma compositions

The spatial geochemical variation from NE to SW in the NTVZ volcanic rocks, expressed as an increase in K_2O content, reduction in SiO_2 content, and LILE and LREE enrichment (Figs 3 and 7a), suggests increasing involvement of an enriched mantle source component or decreasing degrees of partial melting in the petrogenesis of the most primitive mafic magmas. In terms of the Sr–Nd–Pb isotope compositions (Figs 8 and 9), however, they do not show any systematic spatial variation. For instance, the KYS magmas have the second highest contents of K_2O, LILE and LREE among the NTVZ (lower only than the highest TLS magmas; Figs 5, 6 and 7a), whereas they have relatively higher Nd and lower Sr isotope ratios compared with the other NTVZ volcanic rocks (Fig. 8). Thus, the Nd–Sr isotope composition of the NTVZ volcanic rocks does not support a

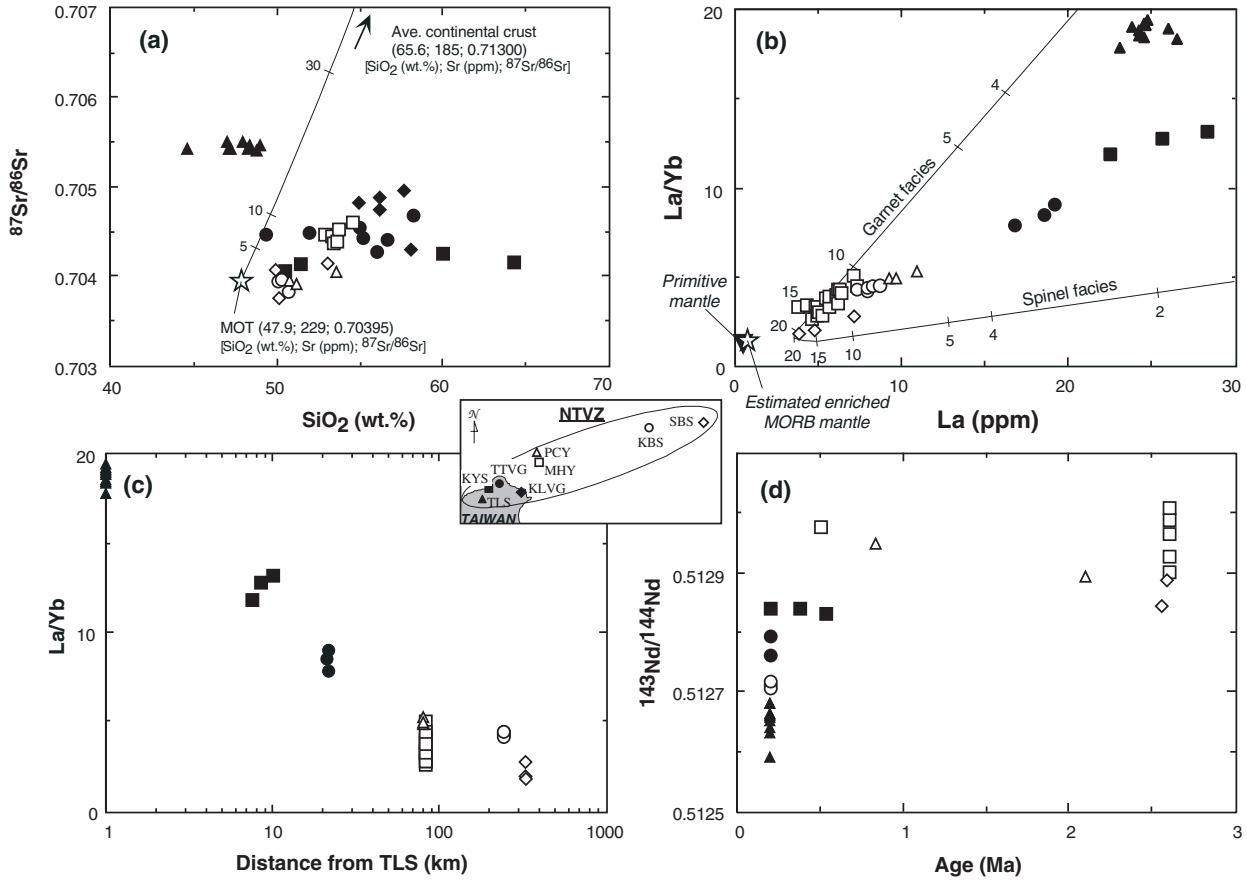

Fig. 10. (a) $^{87}Sr/^{86}Sr$ vs SiO_2 (wt %) for the NTVZ volcanic rocks. Compositions of average Taiwan continental crust and the MOT basalt are from Lan *et al.* (1990) and Wang (1998), respectively. Numbers in the diagram indicate the percentage of crustal contamination. (b) La/Yb vs La for the NTVZ volcanic rocks. Continuous lines are model curves for partial melting of enriched MORB-source mantle, estimated from basalts in MOT (Wang, 1998), with spinel-facies and garnet-facies mineralogy. Ticks with a number represent the degree of partial melting. Values used in modelling are shown in Table 3. The assumed melting model is non-modal batch melting. It should be noted that variation in La/Yb for the NTVZ may result from change in the degree of partial melting. The composition of primitive mantle (Sun & McDonough, 1989) is shown for comparison. (c) La/Yb vs distance from the TLS of each of the NTVZ volcanic fields. Distances are calculated horizontally from the location of the TLS. Because of the logarithmic scale, the distance of the TLS is unity. (d) Eruption ages vs $^{143}Nd/^{144}Nd$ for the NTVZ volcanic rocks.

southwesterly increasing involvement of an enriched source component.

The La/Yb ratios in the NTVZ mafic rocks increase with La concentration (Fig. 10b) and also with NE to SW progression (Fig. 10c). This increase in the La/Yb ratios could not result from increased involvement of an enriched mantle source component because there is no supporting evidence from the Nd–Sr–Pb isotope compositions. The La/Yb variation trend plots within that defined by partial melting of a local enriched MORB mantle source estimated for the MOT in the garnet and spinel facies (Fig. 10b; Table 3) and is not controlled by amount of the residual garnet. Consequently, the degree of partial melting in the NTVZ mantle source may play the dominant role in this chemical variation.

The geochemical characteristics of the NTVZ volcanic rocks show not only a spatial variation but also a change with eruption age. Older (~2·8–2·6 Ma) volcanic rocks from the SBS and MHY are low-K (Fig. 3a), followed by the dominantly calc-alkaline series of the PCY and TTVG (~2·1–0·2 Ma), then finally by the recent (≤0·2 Ma) high-K to shoshonitic volcanism of the KBS, KYS and TLS. The earliest SBS and MHY magmas have the lowest LILE and LREE abundances, whereas the youngest KYS and TLS magmas are extremely enriched in LILE and LREE. The PCY and TTVG magmas erupted at an intermediate time and show transitional abundances of the trace elements (Fig. 7a). The $^{143}Nd/^{144}Nd$ ratios of the earliest SBS and MHY magmas extend up to 0·51301; however, the youngest TLS magmas have the lowest $^{143}Nd/^{144}Nd$ ratio of 0·51260. Figure 10d shows that the highest Nd isotopic ratios occur in the earlier NTVZ magmas, and vice versa. These data indicate that in the mantle source region an

Table 3: Values used in modelling the degree of partial melting

	Spinel peridotite		Garnet peridotite	
	Source mode (X)	Melting mode (Pi)	Source mode (X)	Melting mode (Pi)
Ol	0·53	−0·4	0·6	0·1
Opx	0·27	0·3	0·2	0·18
Cpx	0·17	0·9	0·1	0·3
Spinel	0·03	0·2		
Garnet			0·1	0·42
Ref.	1	2	1	2

	Bulk *D*	Melt mode (P)	Bulk *D*	Melt mode (P)	Estimated E-MORB mantle conc.
Nb	0·0026	0·0109	0·0025	0·0074	0·5
La	0·0101	0·0496	0·0062	0·0171	0·74
Tb	0·0772	0·3976	0·1660	0·6373	0·15
Yb	0·0962	0·3897	0·7050	2·8262	0·67
Ref.	3		3		4

1, Johnson (1998); 2, Kelemen *et al*. (1993); 3, Pearce & Parkinson (1993) and Halliday *et al*. (1995); 4, estimated from basalts in Middle Okinawa Trough (MOT; Wang, 1998; Shinjo *et al*., 1999) assuming the degree of partial melting is 15%.

enriched component became more important in the generation of the younger NTVZ magmas. In summary, the spatial variation of the NTVZ volcanic rocks reflects differences in the degrees of partial melting, whereas their isotopic change with time suggests changes in compositions of the mantle source components beneath the NTVZ.

Mantle source components

The asthenospheric mantle and subcontinental lithospheric mantle (SCLM) source components

The MHY and TLS magmas are the most two primitive melts in the NTVZ, which might shed light on the mantle source components. The TLS magmas are highly magnesian (MgO ≈ 15 wt %; Mg number ≈ 80–83) and potassic (K_2O ≈ 5 wt %; K_2O/Na_2O ≈ 1·6–3·0) with enriched LILE and LREE contents but relatively low basaltic components (i.e. Al_2O_3 ≈ 12 wt %, total Fe_2O_3 ≈ 7·5 wt % and CaO ≈ 7·5 wt %). They have the lowest Nd and highest Sr isotopic ratios among the NTVZ. Their overall geochemical characteristics are comparable with those of the Group I ultrapotassic rocks defined by Foley *et al.* (1987), such as orogenic lamproites from central Italy, Spain and Tibet. On this basis, Chung *et al.* (2001*b*) suggested that the TLS magmas resulted from partial melting of a phlogopite-bearing harzburgitic source in the SCLM that underwent a recent metasomatism by subduction-derived fluids. Thus, an enriched SCLM is one of the potential mantle source components for the NTVZ volcanic rocks. The TLS Nd model ages also strongly suggest an SCLM origin. Nd model ages ranging from 2·0 to 2·5 Ga are consistent with Re–Os model ages for sulphides in peridotite mantle xenoliths entrained by the MTIB (T_{RD} ≈ 1·9 ~2·3 Ga; Wang *et al.*, 2003) indicating the presence of Proterozoic SCLM domains beneath northern Taiwan. On the other hand, the MHY magmas have high MgO contents (≈ 5·9–8·1 wt %, Mg number ≈ 0·6) relative to SiO_2 (≈ 52·8–54·5 wt %), with moderate enrichment in LILE and LREE but no apparent HFSE depletion (Fig. 7b). They have high basaltic components (i.e. CaO ≈ 7·7–8·5 wt %, total Fe_2O_3 ≈ 10·2–11·8 wt % and TiO_2 ≈ 1·4–1·8 wt %) reflecting a fertile mantle source. Although their elevated SiO_2 contents (≈ 52·8–54·5 wt %) could indicate fractional crystallization, the high-Mg characteristics of the MHY magmas suggest a primitive nature for these silica-saturated magmas (Wang *et al.*, 2002). These high-Mg basaltic andesites have the highest Nd isotope ratios and relatively elevated Sr isotopic ratios. The geochemical characteristics of the MHY magmas are similar to those of the MTIB magmas in northwestern Taiwan (Chung *et al.*, 1994, 1995*a*) and almost the same as those of high-Mg andesites from Iriomote-jima, southern Ryukyus (Shinjo, 1999; Fig. 7b); both are considered to be examples of intra-plate volcanism caused by extensional tectonic activity on the Asian continental margin in the Miocene. Similar to the most depleted SCS and NTIB samples (Tu *et al.*, 1992; Chung *et al.*, 1994, 1995*a*), the MHY lavas have high Nd isotopic ratios ($^{143}Nd/^{144}Nd$ ≈ 0·51290–0·51301), which suggest a similar mantle source to the local enriched asthenospheric mantle. This source is not the same as the SCLM that produced the TLS magmas. It is also difficult to ascribe the MHY magmas to an SCLM source because such a source with a Nd isotopic ratio of up to ~0·51301 is probably too refractory to produce the high degree of partial melting required for the MHY magmas (Fig. 10b). Thus, Wang *et al.* (2002) suggested that the MHY magmas were derived from an asthenospheric mantle source with E-MORB characteristics. The high Sr isotopic ratios ($^{87}Sr/^{86}Sr$ ≈ 0·70438–0·70453; Wang *et al.*, 2002) of the MHY magmas are inferred to be derived by fluxing of aqueous slab fluids with no sedimentary components into the mantle source region. This process is analogous to that suggested for the petrogenesis of some island arc tholeiites in the South Sandwich and the Izu–Bonin–Mariana arcs (e.g. Pearce *et al.*, 1995; Taylor & Nesbitt, 1998).

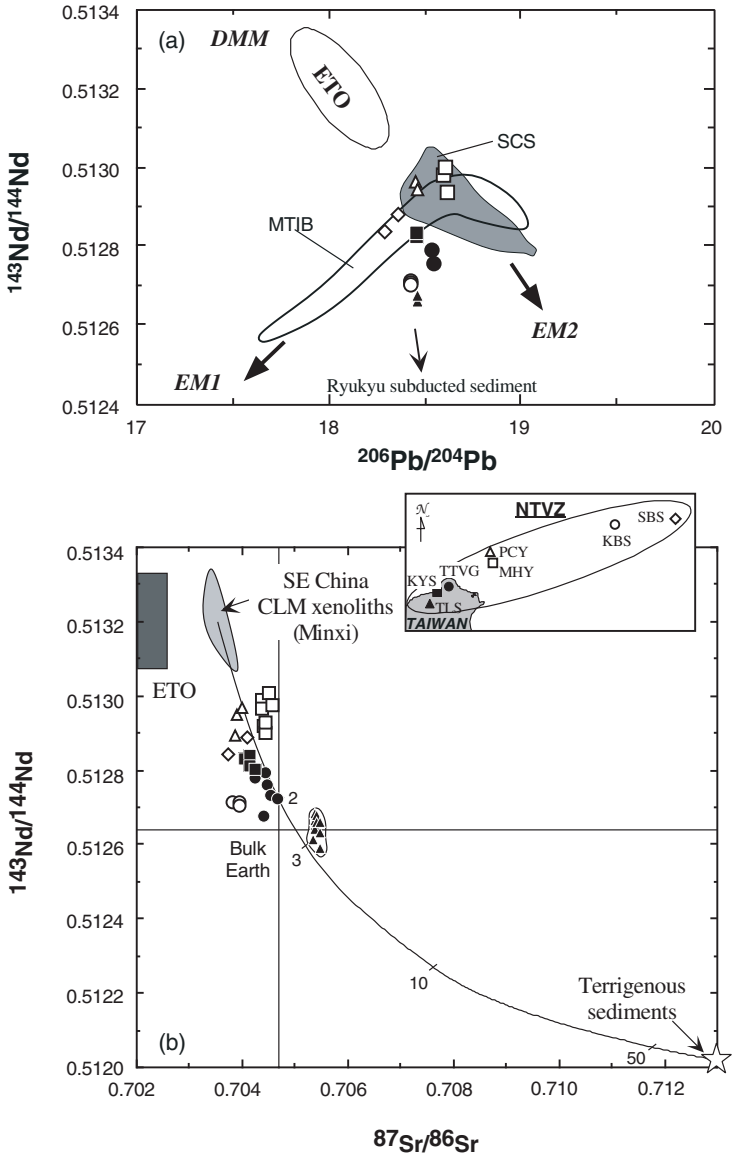

Fig. 11. (a) $^{143}Nd/^{144}Nd$ vs $^{206}Pb/^{204}Pb$ for the NTVZ volcanic rocks. A sedimentary component is revealed in the mantle source region of the NTVZ magmas. Data sources are the same as in Figs 8 and 9. (b) $^{87}Sr/^{86}Sr$ vs $^{143}Nd/^{144}Nd$ for the NTVZ volcanic rocks showing the composition of the metasomatized SCLM. Mixing the average value of the isotope composition of xenoliths from Minxi, southeastern China (Tatsumoto *et al.*, 1992), which are considered to represent the original SCLM beneath Taiwan, with 3% subducted terrigenous sediments can produce the isotope composition of the TLS magmas.

Subduction components

The inferred mantle source components for the NTVZ magmas, the SCLM and the asthenospheric mantle, are both interpreted to be metasomatized by subduction components. In terms of Sr–Nd–Pb isotope compositions (Figs 8, 9 and 11a), the involvement of a sedimentary component in the mantle source region for the NTVZ magmas is strongly indicated. Using mantle xenoliths entrained within the Miocene intra-plate basalts in northwestern Taiwan and southeastern China as samples of the SCLM with no recent subduction metasomatism, mixing calculations based on their Nd–Sr isotope compositions show that 3% subducted sediments would need to be added to the unmetasomatized SCLM to yield a possible source for the TLS magmas (Table 4; Fig. 11b). A depleted mantle source infiltrated by varying amounts of sediment-derived melts may explain the compositional trend for the NTVZ magmas in the Nd–Sr and Pb–Pb isotope diagrams (Figs 8 and 9). However, there is no systematic Sr–Nd–Pb isotopic variation within the NTVZ distribution paralleling the present-day Ryukyu Trench and a variable

Table 4: Values used in mixing calculation between mantle source components

	Nd (ppm)	Sr (ppm)	$^{143}Nd/^{144}Nd$	$^{87}Sr/^{86}Sr$	Nb/U	Ce/Pb	Ref.
E-MORB (P-ETO)	9·82		0·51309		46·1	25	1
Slab-derived fluid	10·00		0·51320		0·155	0·1125	2
Terrigenous sediments	33·00	185	0·51202	0·71300	8·93	3·2	3
Mantle xenoliths (av.)	0·98	27	0·51320	0·70355			4
TLS (av.)	24·24	705	0·51265	0·70545			
MHY (av.)	8·72	210	0·51296	0·70308*			5

1, Sun *et al*. (1979), Sun (1980) and Jahn (1986); 2, Tatsumi and Kogiso (1997) and Ayers (1998); 3, Lan *et al*. (1990); 4, Tatsumoto *et al*. (1992); 5, *using E-MORB values (Sun *et al*., 1979) (see text for explanation).

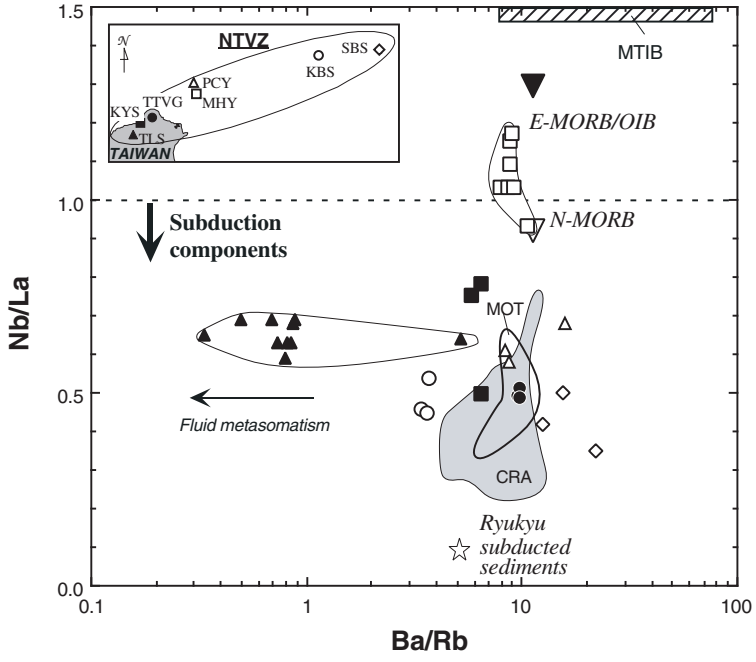

Fig. 12. Nb/La vs Ba/Rb for the NTVZ volcanic rocks. Values of N-MORB (normal MORB), E-MORB and OIB are from Sun & McDonough (1989). Other data sources are the same as in Figs 8 and 9.

sediment flux into the mantle source is difficult to conceive. In addition, the high Nd and Sr isotopic ratios for the MHY magmas and specific incompatible element ratios in the TLS magmas, e.g. Nb/U $\approx$ 0·8, Ce/Pb $\approx$ 2, Rb/Cs $\approx$ 8 and Ba/Rb $\approx$ 1, are not consistent with simple source sediment contamination. Chung *et al.* (2001*b*) suggested that another type of non-magmatic enrichment is required. On the basis of mineral–aqueous aqueous fluid experiments (Keppler, 1996; Tatsumi & Kogiso, 1997; Ayers, 1998), we suggest this enrichment agent to be a hydrous fluid derived from the subducting slab. The distinction between sediment melt and slab-derived fluid is clearly shown by a Nb/La vs Ba/Rb plot (Fig. 12).

Whereas the MHY magmas, with their distinct E-MORB affinity (Nb/La $\geq$1), reflect an origin from an asthenospheric source, the TLS and other NTVZ volcanic rocks with Nb/La $<$1 can be interpreted to be derived from an SCLM altered by subduction-related metasomatism. The TLS magmas have extremely low Ba/Rb ratios, which indicate fluid-dominated metasomatism of the source rather than sediment melting as shown by the other NTVZ volcanic rocks. As the slab-derived fluid has similar $^{143}Nd/^{144}Nd$ ratios to MORB but with unique specific trace-element ratios, and the sediment melt displays lower $^{143}Nd/^{144}Nd$ ratios with different trace-element ratios, plots of Nb/U and Ce/Pb vs $^{143}Nd/^{144}Nd$ can discriminate the extent of

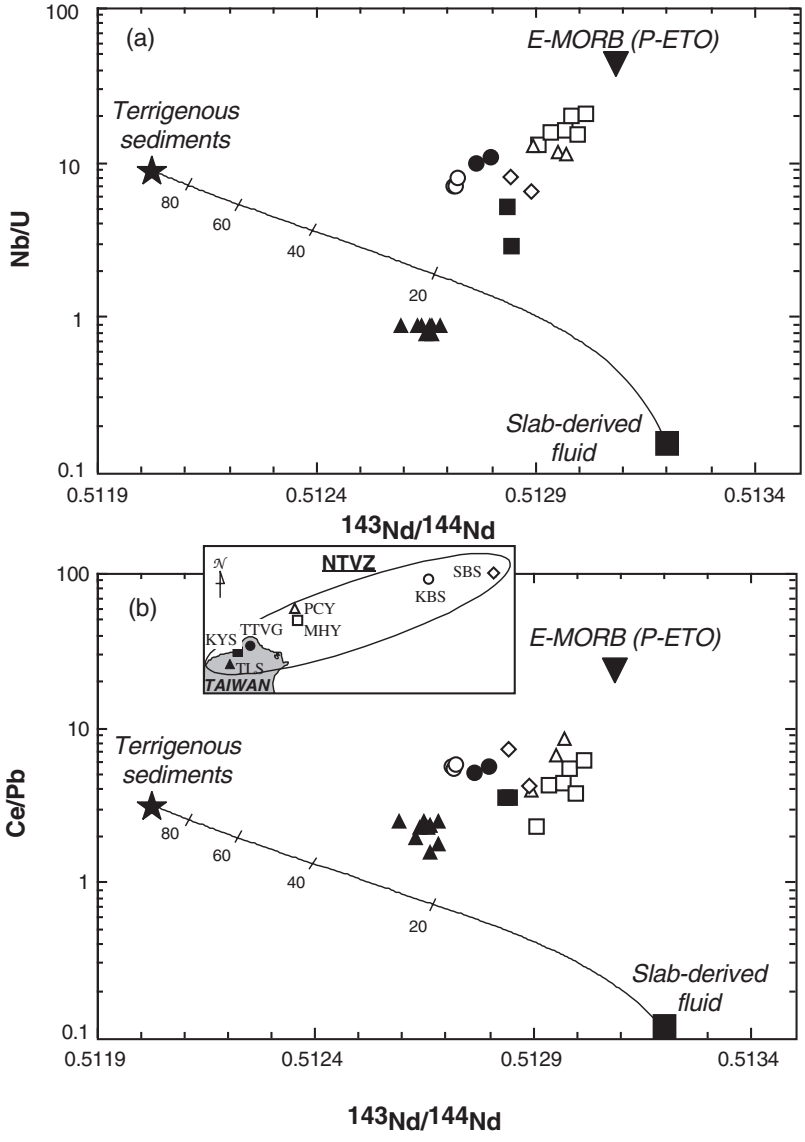

Fig. 13. Nb/U (a) and Ce/Pb (b) vs $^{143}Nd/^{144}Nd$ for the NTVZ volcanic rocks. Data for enriched-type ETO (P-ETO) are from Sun *et al.* (1979), Sun (1980) and Jahn (1986). Small ticks with numbers on the mixing curve between the slab-derived fluid (Tatsumi & Kogiso, 1997; Ayers, 1998) and terrigenous sediment (Lan *et al.*, 1990) indicate percentages of sedimentary components. Compositions used in mixing calculation are shown in Table 4. In comparison with the TLS lavas, which plot close to the mixing curve, most NTVZ rocks plot between the mixing curve and an E-MORB mantle source.

involvement of both subduction components in the metasomatism (Table 4; Fig. 13).

The average composition of the continental sediments on Taiwan was chosen to represent that of the subducted terrigenous sediments (Lan *et al.*, 1990) because of the active NW subduction of the Philippine Sea plate along the eastern margin of the Taiwan orogen. Compositions for the slab-derived fluid were taken from Tatsumi & Kogiso (1997) and Ayers (1998). Using P-type (enriched) ETO as a starting material representing local enriched MORB mantle source unmodified by recent subduction metasomatism, mixing calculations show that all the NTVZ volcanic rocks plot along a mixing trend between the P-ETO and TLS (Fig. 13). A fluid-dominated metasomatism coupled with a 20–30% contribution from average terrigenous sediment is also shown in the TLS mantle source region that lies close to the mixing line between the average terrigenous sediment and the slab-derived fluid. The fluid-dominated metasomatism may have resulted in a phlogopite-bearing harzburgitic mantle (Wyllie & Sekine, 1982). Such a mantle has a substantially lower solidus temperature than refractory SCLM, and could be preferentially partially melted during the initial stages of thermal perturbation owing to extension.

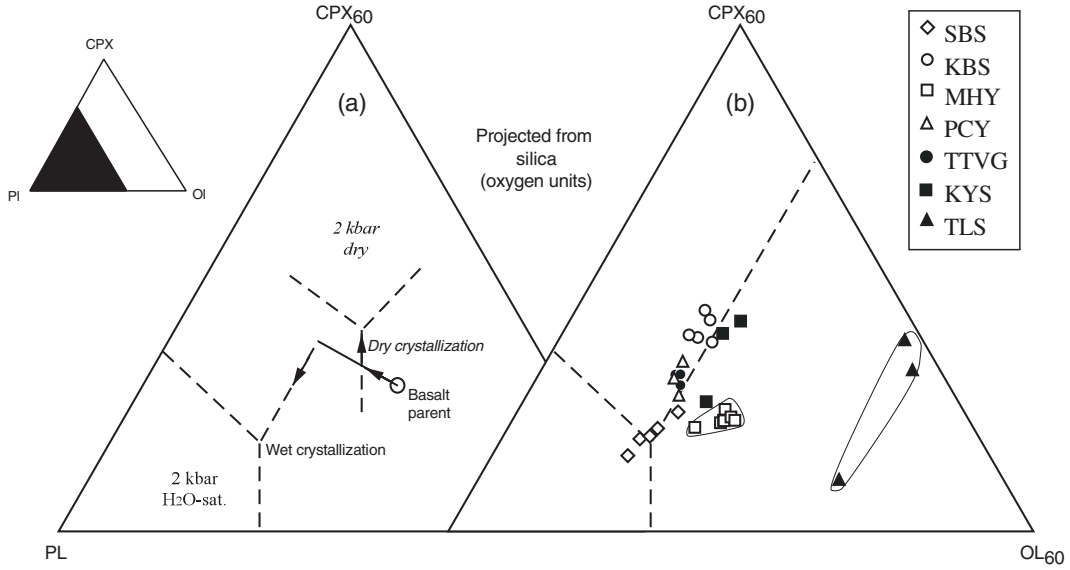

Fig. 14. (a) Schematic liquid lines of descent for a primitive basalt under hydrous and anhydrous conditions. (b) Compositions of the NTVZ volcanic rocks. It should be noted that there are different eutectic points and paths of fractional crystallization for parental basaltic magmas under anhydrous and hydrous conditions. Diagrams are modified from Gaetani *et al.* (1993).

Other evidence for fluid-dominated metasomatism of the mantle source might come from generation of high-Al basalts in the NTVZ. High-Al basalts have been considered to be primary melts from large degrees (~50–60%) of partial melting of eclogites in subducting plates (e.g. Brophy & Marsh, 1986; Myers *et al.*, 1986). However, considering the difficulty of deriving large-degree partial melts from the old and cold subducting Philippine plate (~45 Ma) in the Ryukyu subduction system, high-Al basalts in the NTVZ are most likely to be the result of fractional crystallization rather than representing primary melts. Alternatively, Gaetani *et al.* (1993) pointed out that the presence of water in the mantle wedge above a subduction zone can significantly alter the compositional path followed by residual liquids, and modify the types and compositions of crystals that accumulate at the site of cooling. Accordingly, under hydrous conditions, early crystallization of plagioclase is suppressed so that aluminium contents in residual liquids increase to yield high-Al basalts (Fig. 14a). Figure 14b shows that most of the NTVZ volcanic rocks lie along the olivine–clinopyroxene cotectic for hydrous crystallization. This suggests that their mantle source region might be hydrous. The SBS lavas, all high-Al basalts, plot closest to the olivine–clinopyroxene–plagioclase ternary eutectic, indicating that high-Al basalts in the NTVZ are not primary melts but have undergone some fractional crystallization.

In comparison with the MTIB in northwestern Taiwan erupted prior to the Taiwan arc–continent collision (Chen, 1990; Chung *et al.*, 1995*b*), the NTVZ magmas with subduction-modified geochemical characteristics suggest that the upper mantle domain underwent metasomatism related to subduction zone processes during the buildup of the NTMB. Considering the tectonic evolution of Taiwan region since arc–continent collision at ~10 Ma (e.g. Teng, 1990), the Ryukyu subduction system is the only one that approached the northern Taiwan region and was most likely to cause the required metasomatism. Most NTVZ volcanic rocks having geologically meaningless negative Nd model ages may also result from this recent metasomatism.

The mixing of mantle source components and partial melting conditions

The mixing trend in Fig. 13 also suggests that mixing of partial melts of enriched asthenospheric mantle and subduction-metasomatized SCLM could explain the geochemical characteristics of the NTVZ volcanic rocks. Although the MHY magmas have lower values than the P-ETO, they still plot at the other end of the mixing trend (Fig. 13a). The MHY mantle source might have been fluxed by slab-derived fluid but not sediment melts, so their Ce/Pb ratios are much lower (Fig. 13b). The effect from the slab-derived fluid is not clear for Nb/U probably because the MHY magmas have higher Nb contents similar to E-MORB. A similar mixing trend is observed in the Nd–Sr isotope diagram (Fig. 8), in which the other NTVZ volcanic rocks lie along a mixing trend between the depleted MHY and enriched TLS mantle sources despite the elevated Sr isotopic ratios of the MHY magmas. A simple source sediment contamination model is not preferred because variable sediment flux in the

NTVZ mantle sources unrelated to NTVZ distribution would be highly unlikely to lead to systematic isotopic variation among the NTVZ. Alternatively, we propose that variable mixing of melts from the depleted asthenospheric mantle at the site of formation of the MHY magmas, and the subduction-metasomatized SCLM where the TLS magmas formed could satisfy most of the geochemical characteristics of the NTVZ magmas. The proportions of the melts from the metasomatized SCLM mixing with asthenospheric melts can be calculated based on the NTVZ Nd–Sr isotopic ratios: 12–17% for the SBS, ~20% for the KBS, ~13% for the PCY, ~30% for the TTVG and ~20% for the KYS, respectively (Fig. 8), using compositions of the MHY and TLS magmas as the two end-members. In the calculation, the most enriched Sr isotope value of E-MORB ($^{87}Sr/^{86}Sr = 0{\cdot}70308$; Sun *et al.*, 1979) instead of that of the MHY magmas was used because the MHY magmas have elevated Sr isotope ratios as a result of subduction-fluid flux. The degree of partial melting also plays an important role in controlling the spatial geochemical variation among the NTVZ, which the simple source sediment contamination model can not decipher.

The mantle xenoliths entrained within the MTIB are dominantly refractory harzburgites (Yang *et al.*, 1987), so this part of the SCLM is not a productive magma source. Whereas the fluid-dominated metasomatism substantially lowers the solidus temperature of the refractory SCLM, the TLS magmas, indicative of the most fluid-dominated metasomatized SCLM source, still show extremely low degrees of partial melting. Using the Batan sub-arc phlogopite-bearing harzburgites from the Philippines (Maury *et al.*, 1992) (which are the analogue of the TLS mantle source and generated similarly high-K magmas) as the starting source material in the graphical concentration ratio (CR) method of Maaloe (1994), <2% of partial melting is estimated for the TLS magmas (Table 3; Fig. 15). Thus, except for the MHY and TLS magmas, which are separately derived from the asthenospheric and lithospheric mantle, most of the NTVZ magmas are the products of variable degrees of partial melting of asthenospheric mantle, variously 'contaminated' by melts from the metasomatized SCLM during ascent.

The degrees of partial melting for the NTVZ can be evaluated by the CR method using an enriched MORB mantle source as the starting source material, which is estimated from basalts in the MOT with a subduction flux similar to that for the MHY magmas (Table 3; Fig. 15). We suggest that the parental magmas of the offshore volcanic fields in the NTVZ were generated by larger degrees of partial melting (8–20%) than the onshore fields (2–5%). A southwestward decrease in degree of partial melting is also revealed, which is evident in the plot using dominantly mantle-derived elements or conservative elements (e.g. Nb and Yb; Pearce & Parkinson, 1993; Pearce & Peate, 1995) without significant subduction contribution (Fig. 15b). The degrees of partial melting of the asthenospheric source may depend on both the overlying lithospheric thickness (the minimum depth at which the melting occurred) and the specific mantle domain composition. The latter cause is not preferred here as the isotopic characteristics of the NTVZ magmas are decoupled from the inferred degree of partial melting. In addition, the overlying lithospheric thickness also determines the extent to which the metasomatized SCLM contaminated the asthenospheric melts. In the NTVZ, the spatial and temporal changes in magma composition, reflecting lithosphere architecture and history within a coherent tectonic terrane, allow some important inferences to be made about the geodynamic evolution of this complex region (see next section), and also about the variable nature of the lithosphere traversed by the mantle-derived mafic magmas in time and space.

Petrogenetic model

To test our hypothesis, modelling of trace-element concentrations in the mantle sources and melts was carried out. Non-modal batch melting was assumed and the compositions of the mantle sources for the MHY and TLS magmas were used as starting points. As Wang *et al.* (2002) suggested that asthenospheric mantle ascended to ~60–70 km depth to generate the MHY magmas at ~2·6 Ma, we assume that all melts, including the TLS melts from the SCLM, occur in the garnet stabilizing field of the mantle. Using the trace-element partition coefficients of Halliday *et al.* (1995), Johnson (1998) and Schmidt *et al.* (1999), the trace-element compositions of the MHY and TLS mantle sources were calculated from the average lava compositions using the estimated degrees of partial melting shown in Fig. 15 (8% for the MHY and 2% for the TLS), and appropriate source and melt modes (garnet lherzolites for the MHY and phlogopite–garnet harzburgites for the TLS; see Table 5 for details). Having thus established the trace-element compositions of the enriched asthenospheric and metasomatized SCLM source components, the trace-element composition of the asthenospheric melts can be derived for the individual NTVZ volcanic fields. Finally, a simple mixing calculation based on the estimated compositions of the asthenospheric melts and those from the metasomatized SCLM, using the proportions shown in Fig. 8 for the individual NTVZ volcanic fields, provides their model trace-element compositions. The model trace-element compositions are plotted in Fig. 16 compared with the actual compositions of the NTVZ magmas (except for the MHY and TLS magmas used as end-members). Although the model compositions for the NTVZ do not perfectly coincide with their actual values in Fig. 16, the geochemical variation trends of

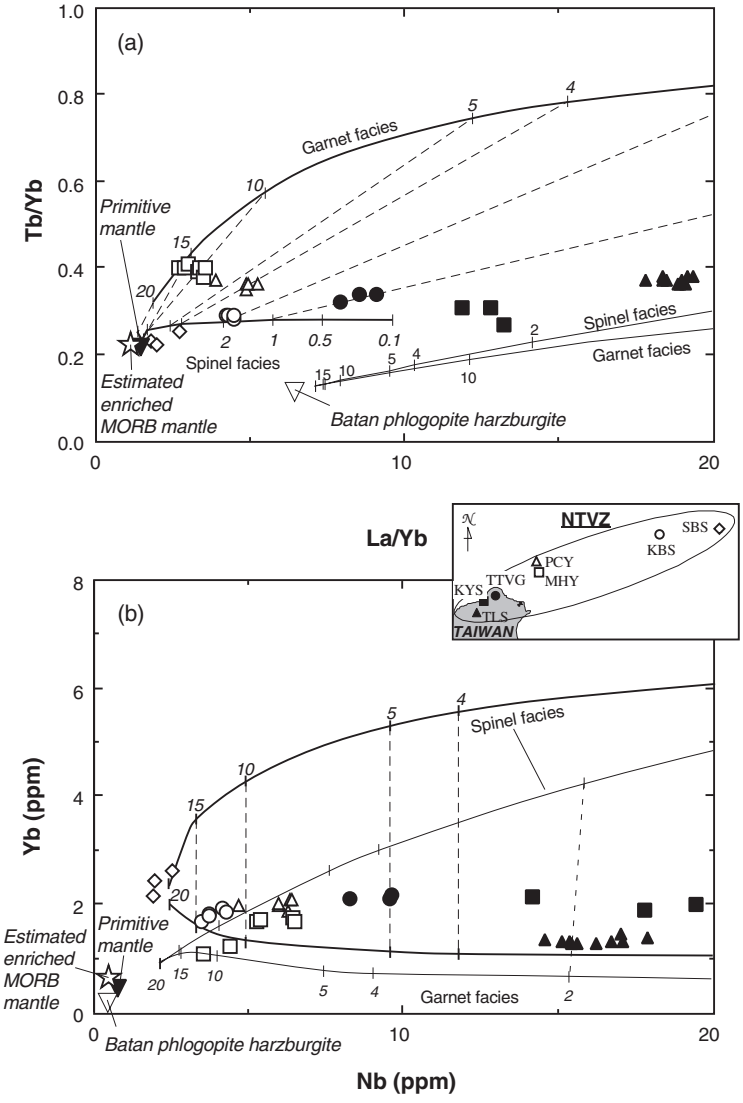

Fig. 15. Variation of (a) Tb/Yb vs La/Yb and (b) Nb vs Yb for the NTVZ volcanic rocks. Bold continuous lines are model curves for partial melting of the enriched MORB mantle, estimated from basalts in MOT (Wang, 1998), with spinel-facies and garnet-facies mineralogy. Dashed lines connect the same degree of partial melting between the two facies. Fine continuous lines are model curves for partial melting of Batan phlogopite harzburgite (Maury *et al.*, 1992), an analogue of the TLS mantle source, with spinel-facies and garnet-facies mineralogy. Small ticks with numbers represent the degrees of partial melting. Values used in modelling (Table 3), the melting model and distribution coefficients are the same as in Fig. 10b. The primitive mantle (Sun & McDonough, 1989) is shown for comparison.

the NTVZ magmas are successfully modelled by this method.

GEODYNAMIC MODEL

Wang *et al.* (1999) proposed that the magmatism of the northern Taiwan volcanic zone resulted from post-collisional extension in the NTMB since Plio-Pleistocene times. Initiation of the NTVZ thus serves as a straightforward constraint for the onset of the collapse of the NTMB. Whereas structural and seismological data (Suppe, 1984; Lee & Wang, 1988; Yeh *et al.*, 1991) provide lines of evidence for post-collisional extension in the Quaternary, a geodynamic model for the tectonic evolution accommodating seismological and geophysical data is still unavailable. This is especially the case when the NTVZ is considered not to be part of the Ryukyu Arc. Using analogies from other localities of Tertiary post-collisional magmatism, e.g. Tibet, China (e.g. Turner *et al.*, 1996; Maheo *et al.*, 2002) and the Betic–Alboran domain of SE Spain (Turner *et al.*, 1999), we suggest a geodynamic model for the post-collisional extension based on our interpretation of the NTVZ geochemical data.

Table 5: Values used in trace-element modelling

	Garnet peridotite		Phlogopite–garnet harzburgite	
	Source mode (X)	Melting mode (Pi)	Source mode (X)	Melting mode (Pi)
Ol	0·6	0·1	0·6	0·05
Opx	0·2	0·18	0·2	0·32
Cpx	0·1	0·3		
Garnet	0·1	0·42	0·1	0·4
Phl			0·1	0·23
Ref.	1	2		

	Bulk *D*	Melt mode (P)	Bulk *D*	Melt mode (P)	MHY (av.)	TLS (av.)
Nb	0·0025	0·0074	0·0081	0·0199	5·98	16·12
La	0·0062	0·0171	0·0011	0·0020	5·58	24·68
Sm	0·0503	0·1742	0·0239	0·0906	2·96	4·59
Zr	0·0490	0·1643	0·0360	0·1138	78·86	117·51
Y	0·2549	0·9845	0·2109	0·8121	19·71	14·61
Yb	0·7050	2·8262	0·6650	2·5803	1·52	1·32
Ref.	3		1, 3, 4			

1, Johnson (1998); 2, Kelemen *et al*. (1993); 3, Halliday *et al*. (1995); 4, Schmidt *et al*. (1999).

Models involving a retreating subduction zone (e.g. Lonergan & White, 1996), slab detachment or break-off (e.g. Davies & von Blankenburg, 1995), delamination (e.g. Bird, 1979) and convective removal of the lithosphere (e.g. Houseman *et al.*, 1981) have been used to explain post-collisional extension. All these processes cause upwelling of the asthenosphere and this will perturb the original thermal gradient. Consequences that follow are magma generation and sequential extension. Combining the magmatic history with other constraints based on the tectonic evolution of an area may lead to a more robust dynamic model (e.g. Turner *et al.*, 1999).

Relative to the present-day location of Taiwan, the initial arc–continent collision started in the NE at ~10 Ma and propagated southwestward corresponding to the relative motion between the Philippine and Eurasian plates (Suppe, 1984). According to the sedimentary record (Teng, 1990), the collision activity was most intensive at ~6–5 Ma, resulting in an uplift of nearly 4000 m above sea level (Fig. 1). Meanwhile, both the arc and associated back-arc volcanism in the middle part of Ryukyu subduction experienced a hiatus in the period of 6–2 Ma (Letouzey & Kimura, 1986; Kamata & Kodama, 1994; Park, 1996). This indicates a feedback relationship between the Taiwan collision and the development of the part of the Ryukyu subduction system near northern Taiwan.

Severe compressional forces near the northern Taiwan region probably stalled the Philippine Sea plate subduction so this slab could not encroach beneath the region. Consequently, the Ryukyu subduction re-established and re-generated arc and back-arc volcanism at a later stage. Two phases of the Okinawa Trough opening at 10–6 and ~2 Ma (Miki, 1995; Sibuet *et al*, 1998) may respond to the re-establishment of the Ryukyu subduction system. The thickened lithosphere caused by arc–continent collision would have also prevented western propagation of the Ryukyu subduction system (Fig. 17a). This model differs from previous ones suggesting that the Ryukyu subduction zone was able to continue developing in the northern Taiwan region (Chen, 1990; Teng *et al.*, 1992; Teng, 1996).

Several lines of evidence also support the interpretation that the NTVZ is unlikely to be part of the Ryukyu Arc. They include a horizontal displacement (of about 150 km) from the western end of the actual Ryukyu volcanic arc (Iriomotejima; Fig. 1) to the NTVZ, and the fact that the north-dipping Benioff zone of the subducting Philippine Sea plate is now sitting ~200–250 km beneath the NTVZ (Eguchi & Uyeda, 1983; Kao *et al.*, 1998) compared with ~100 km for the normal Ryukyu Arc. There are apparent differences in the duration of volcanism between the NTVZ and the Ryukyu Arc, as the latter became dormant in the earliest Pliocene (Shinjo, 1998). In terms of their geochemical characteristics, if the NTVZ magmas represent arc volcanism, their systematic along-arc (spatial) geochemical variations (reflecting systematic variable degrees of partial melting in their mantle source) should represent a typical cross-arc variation for the arc volcanism. This is not supported by the actual spatial distribution of the NTVZ paralleling the Ryukyu Trench. Moreover, the along-arc variation is also difficult to ascribe because there is no apparent spatial variation in the subducting plate, i.e. sediment flux etc., if the NTVZ is treated as arc-related volcanism. As there was no active subduction near northern Taiwan during that time, tectonic models involving a retreating subduction zone and slab detachment or break-off models cannot be realistic for the NTVZ. However, metasomatism by the Ryukyu subduction zone could still affect upper-mantle domains beneath northern Taiwan because of the lateral migration of subduction components (Fig. 17a).

The geochemical characteristics of the MHY asthenospheric melts indicate that significant upwelling of asthenosphere to 60–70 km depth has occurred since ~2·6 Ma (Wang *et al.*, 2002) at the time of initiation of the NTVZ activity (Fig. 17b). Taking account of the continental crustal thickness of ~30 km in northern Taiwan (Yeh *et al.*, 1989), emplacement of the MHY magmas

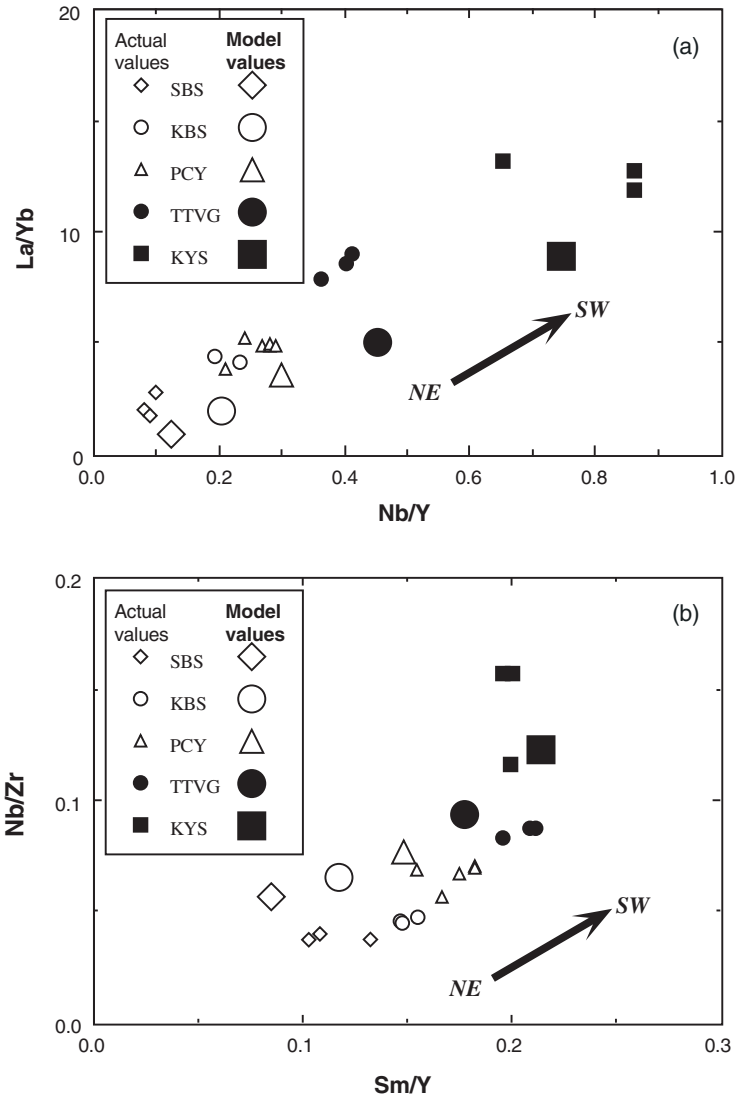

Fig. 16. La/Yb vs Nb/Y (a) and Nb/Zr vs Sm/Y (b) diagrams showing similarities between model and actual ratios in the NTVZ volcanic rocks.

suggests that part of the SCLM was removed or thinned to let the underlying asthenosphere upwell to sufficiently shallow depths for decompressional melting to occur. Because the collision started to the NE of present-day Taiwan close to the MHY, this is inferred to have been the region of thickest lithosphere, and most likely to be removed subsequently, similar to the scenario described for Tibetan post-collisional magmatism by Turner *et al.* (1996). Actually the NTVZ distribution along the underlying northern Taiwan metamorphic basement, which represents parts of the Taiwan orogen and is characterized by folded and tilted Tertiary strata resulting from the collision (Fig. 1; Wageman *et al.*, 1970; also named the southern Taiwan–Sinzi Folded Zone), strongly suggests a link between generation of the NTVZ and collapse of the Taiwan orogen. Seismic profiles show that offshore northeastern Taiwan has been characterized by high-angle normal faults, which have been reactivated from pre-existing, collision-induced reverse faults, since late Pliocene times (Hsiao *et al.*, 1998; Kong *et al.*, 2000; Fig. 1). On this basis, Teng (1996) proposed that extensional collapse of the NTMB took place in Plio-Pleistocene times. The uplift history revealed by the Taiwan basement rocks and sedimentary accumulation in the foreland basins suggests that there was a major acceleration in the rate of uplift of the arc–continent collision zone and an increase in the sediment accumulation rate at ~3–2·5 Ma, following steady-state uplift since ~8 Ma (Teng, 1990, fig. 8). This supports a model of rapid uplift after parts of the SCLM were removed or attenuated.

The SBS, TTVG and later PCY (~2·1 Ma) magmas show HFSE depletion (Fig. 7a), indicating a likely greater

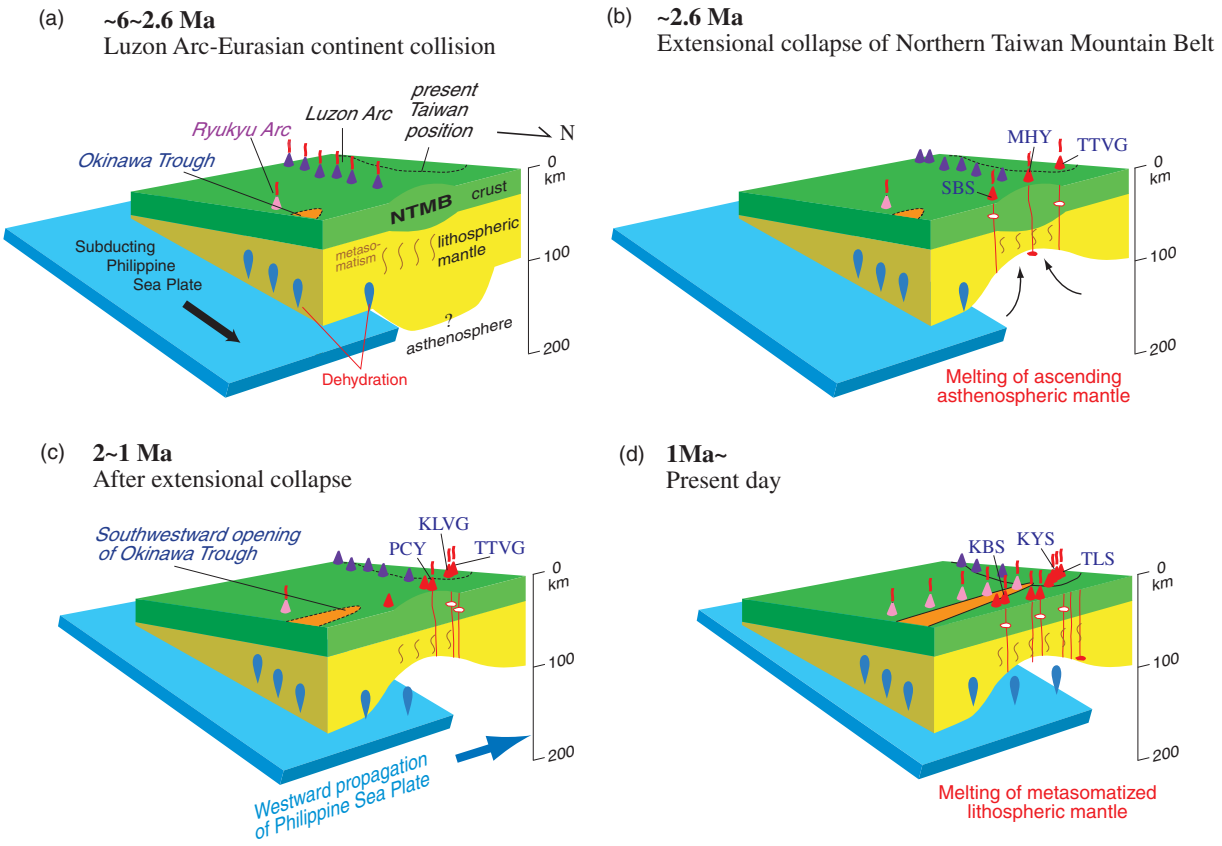

Fig. 17. Schematic representation of the proposed geodynamic model for the NTVZ and related tectonic evolution of the area from ~6 Ma to the present. NTMB, northern Taiwan mountain belt. Volcanoes in different colours indicate different volcanic fields (purple—the Luzon Arc; pink—the Ryukyu Arc; red—the NTVZ); the plumes from volcanoes suggest that the volcanoes are active. (a) The Luzon Arc colliding with the Asian continent formed a thickened SCLM, which prevented the Philippine Sea plate from subducting beneath the northern Taiwan region. Consequently, the Ryukyu Arc and the Okinawa Trough stalled westward propagation. Black dotted line marks the present position of Taiwan. The arc–continent collision started in the NE. (b) As soon as parts of the SCLM were 'removed', asthenospheric mantle upwelled to shallower depth then melted to generate the initial NTVZ volcanism. (c) After parts of the SCLM were 'removed', the Philippine Sea plate started its westward propagation with reopening of the Okinawa Trough towards NE Taiwan to form the SPOT (southernmost part of Okinawa Trough). (d) The SPOT reached to onshore NE Taiwan as the Philippine Sea plate subducted beneath the northern Taiwan region. The subsequent arc volcanism, the western extension of the Ryukyu Arc, was generated in the SPOT, which is located ~80–100 km above the Benioff zone of the Philippine Sea plate.

involvement of subduction components in the metasomatized asthenospheric mantle and/or the SCLM. The SBS and PCY magmas, both offshore and close to the MHY field, are also low-K and calc-alkalic magmas produced by higher degrees of partial melting and with higher $^{143}Nd/^{144}Nd$ ($\approx 0{\cdot}51284$–$0{\cdot}51289$ and $0{\cdot}51289$–$0{\cdot}51297$, respectively). The TTVG magmas are calc-alkaline and have lower $^{143}Nd/^{144}Nd$ ($\approx 0{\cdot}51268$–$0{\cdot}51280$). The correlation might suggest that upwelling of the asthenosphere was shallower offshore, so that higher-degree asthenospheric melts were generated with less contamination by the overlying metasomatized SCLM, and vice versa (Fig. 17b). As a result of the continuing collision in central and southern Taiwan, post-collisional extension induced by asthenosphere upwelling diminished southwestward.

Magmatism during the initial stage of NTVZ activity was dominantly sourced from the asthenospheric mantle (i.e. the MHY, SBS and PCY). These magmas represent higher degrees of partial melting (8–20%) consistent with that predicted from decompressional melting of the ascending asthenosphere up to ~60–70 km depth (10–20%). Some extensive late Pliocene–Quaternary subsurface magmatic fields distributed within the Taiwan orogen basement have been identified on seismic profiles (Fig. 1; Sun & Hsu, 1991; Hsiao *et al.*, 1998). The volume of these subsurface volcanic fields is apparently larger than the NTVZ although no direct age and geochemical data for the magmatic rocks are available. However, it is evident that large amounts of volcanic activity have occurred offshore northeastern Taiwan since the late Pliocene.

After ~2·6 Ma the subducting Philippine Sea plate resumed its westward motion to penetrate progressively into the region beneath the NTMB because parts of the collision-thickened lithosphere that were creating a 'barrier' had been removed (Fig. 17c). Meanwhile, the Ryukyu subduction system developed its southernmost extension corresponding to the movement of the Philippine Sea plate. The reopening of the Okinawa Trough started at ~2 Ma after a hiatus (Letouzey & Kimura, 1986; Park, 1996; Sibuet *et al.*, 1998), and its fast southwestward propagation at ~126 mm/yr reached the I-Lan plain, in NE Taiwan (Liu, 1995) with a very strong curvature. This part of the Okinawa Trough [named SPOT (southernmost part of Okinawa Trough) by Chung *et al.* (2000)] is structurally and geochemically different from its central part. The SPOT back-arc magmas are bimodal andesites and rhyolites, exhibiting typical subduction magma-type characteristics similar to those of the CRA and MOT magmas (Chung *et al.*, 2000). Compared with the MHY magmas with intra-plate geochemical affinities, it is most likely that initial magmatism first occurred within the NTVZ outside the topographical Okinawa Trough, rather than within the trough.

The NTVZ magmas erupted from 2 to 1 Ma consist dominantly of calc-alkalic rocks and display significantly HFSE depletion (Fig. 7a) in contrast to the earlier NTVZ magmas with low-K characteristics. These were widely emplaced at the PCY, KLVG and TTVG localities (Fig. 17c), which extend onshore from an inferred upwelling centre offshore. Greater enrichment in LILE and LREE than the earlier magmas suggests that the proportion of lithospheric components was increasing (Fig. 7a). All phenomena at this stage indicate that subsequent thermal perturbation in the SCLM and the propagation of extension followed asthenospheric upwelling.

The final stages of volcanism show most activity in the KBS, PCY, TTVG, KYS and TLS fields (Fig. 17d) with striking geochemical variations in the magmas. The most recent (~0·2 Ma) magmas at KBS, KYS and TLS have high-K calc-alkaline to shoshonitic–ultrapotassic characteristics with extreme enrichment in LILE and LREE but HFSE depletion (Fig. 7a). The TLS magmas represent an extreme end-member magma type indicative of small-degree partial melts of phlogopite-bearing harzburgitic SCLM. A series of recent volcanic arcs, about 80–100 km above the Benioff zone of the subducting Philippine plate, and representing the western end of the Ryukyu Arc, were formed in the SPOT (Sibuet *et al.*, 1998; Chung *et al.*, 2000). The SPOT is an atypical back-arc spreading setting, which was formed before or at least synchronously with its arc–trench counterpart (Fig. 17d; Wang *et al.*, 1999; Chung *et al.*, 2000). This combination of tectonic and magmatic processes consequently led to a unique collision–extension–subduction context in this region. Sadeghi *et al.* (2000) reported low-velocity anomalies in the uppermost mantle at a depth of 40 km beneath the northern Taiwan region, but beyond the SPOT area, and these might be evidence for the asthenosphere upwelling in the NTMB.

Most models for post-collisional magmatism predict that it should progress from potassic lithosphere-derived melts to intra-plate asthenospheric melts with time (e.g. Pearce *et al.*, 1990; Turner *et al.*, 1992, 1993, 1996; Platt & England, 1993; Maheo *et al.*, 2002). However, Turner *et al.* (1999) reported that post-collisional magmatism in the Betic–Alboran domain in SE Spain exhibits the reverse progression and suggested that this could be due to significant differences in the amount of thickened crust in different collision zones. A general model was proposed for post-collisional magmatism in Tibet where the thickened crust (~70 km) is twice normal thickness. However, the Betic–Alboran domain may not have had such thickened crust, so that the asthenosphere could upwell to higher levels (e.g. less than 50–60 km) after convective removal of some of the thickened lithosphere and thus induce decompressional melting to generate asthenospheric melts first (Turner *et al.*, 1999). Thus, the rheology of both plates in collision, the extent of the collision and the velocity of plate convergence are important controls on the geochemical characteristics and time interval between the onset of collision and the generation of post-collisional magmatism. In the northern Taiwan region we also observe a reverse geochemical pattern for magma suites starting with asthenospheric melts then proceeding to lithospheric melts. The scale of the collision in the Taiwan region is much smaller than that in Tibet, so it is easier to document in detail the different successive magma series within a short time span from the onset of collision in the NTVZ, thus providing constraints for a post-collisional magmatism in a distinctive geodynamic domain similar to that of the Betic–Alboran domain.

CONCLUSIONS

The geochemical characteristics of the NTVZ volcanic rocks indicate that they resulted from the upwelling of asthenosphere in response to post-collisional extension associated with collapse of the NTMB in Plio-Pleistocene times. Their spatial and temporal geochemical variation can be explained and semi-quantitatively modelled by variations in degrees of partial melting, and in the mixing proportions of two dominant end-member source mantle types beneath individual magma fields, which may be distinguished in terms of their geographical location and age of volcanism. The spatial variation of the NTVZ volcanic rocks largely reflects partial melting variations, whereas the changes in isotopic composition with time suggest changes in the compositions of the mantle source components beneath the NTVZ.

The dominant mantle components are the asthenospheric mantle and the SCLM that had undergone metasomatism by subduction processes associated with the Ryukyu subduction system. The subduction-related metasomatism of the SCLM has geochemical characteristics indicating the involvement of both slab-derived fluid and sediment-derived melts that infiltrated the mantle source region of the NTVZ during the build-up of the NTMB. Thus, the 'arc signatures' evident in most of the NTVZ volcanic rocks do not mean that the NTVZ is part of the Ryukyu Arc, as these are not direct melts induced by subduction processes, but extension-induced melts formed significantly after active subduction ceased and that were contaminated by the overlying SCLM (which had inherited subduction components). The retreating subduction zone and slab detachment or break-off models are unlikely to be able to explain the generation of the NTVZ volcanic fields.

It is suggested that the MHY melts represent asthenospheric melting after parts of the thickened lithosphere had been removed (or attenuated) and asthenosphere upwelling took place to shallow depths (~60–70 km). Subsequent emplacement of calc-alkaline magmas indicates increasing involvement of the SCLM in the magma generating process resulting from heating by the newly juxtaposed hotter asthenosphere. Finally the TLS potassic magmas erupted as a result of melting dominantly of the metasomatized SCLM itself. The NTVZ magma series progression is distinct from that predicted by general models for post-collisional magmatism based on the Tibetan post-collisional magmatism, but similar to that of the Betic–Alboran domain. This may be a consequence of the different scales of these collision zones.

ACKNOWLEDGEMENTS

We thank C. Y. Lee and X. H. Li for their help in arranging XRF and ICP-MS analysis, and C.-H. Chen, F. T. Yang and C.-H. Lo at NTU, T. Y. Lee at NTNU, Taiwan, and M. Zhang at GEMOC, Macquarie University, Australia, for thoughtful discussions. Thanks also go to R. Maas of Melbourne University for supplying silica gel–H_3PO_4 solution, and to G. Mortimer of ANU, RSES, for supplying SRM 981 and 982, the ANU double-spike solution and the Excel spreadsheets for double-spike calculation in the early stage of this work. The manuscript was significantly improved by constructive journal reviews from Y. Tatsumi, S. Turner, H. Williams, an anonymous reviewer and the Editor M. Wilson. This study benefited from research grants supported by the National Science Council, Taiwan. Refining of concepts and writing was done while K.-L. Wang was in receipt of a Macquarie University Research Fellowship. This is GEMOC Publication 335.

REFERENCES

Angelier, J., Barrier, E. & Chu, H. T. (1986). Plate collision and paleostress trajectories in a fold–thrust belt: the foothills of Taiwan. *Tectonophysics* **125**, 161–178.

Ayers, J. (1998). Trace element modeling of aqueous fluid–peridotite interaction in the mantle wedge of subduction zones. *Contributions to Mineralogy and Petrology* **132**, 390–404.

Bird, P. (1979). Continental delamination and the Colorado Plateau. *Journal of Geophysical Research* **84**, 7561–7571.

Brophy, J. G. & Marsh, B. D. (1986). On the origin of high-alumina arc basalt and the mechanics of melt extraction. *Journal of Petrology* **27**, 763–789.

Cameron, A. E., Smith, D. H. & Walker, R. L. (1969). Mass spectrometry of nanogram-size samples of lead. *Analytical Chemistry* **41**, 525–526.

Chen, C. H. (1989). Nd–Sr–O isotopic study of Cenozoic arcs volcanic rocks in Taiwan. Ph.D. thesis, National Taiwan University, Taipei, 198 pp. (in Chinese).

Chen, C.-H. (1990). *Igneous Rocks of Taiwan. Central Geological Survey Special Publication* **1**, 137 pp. (in Chinese).

Chen, C. H. (1997). Extensional collapse of the northern Taiwan mountain belt: Comment. *Geology* **25**, 855–856.

Chen, C. H., Shieh, Y. N., Lee, T., Chen, C.-H. & Mertzman, S. A. (1990). Nd–Sr–O isotopic evidence for source contamination and an unusual mantle component under Luzon Arc. *Geochimica et Cosmochimica Acta* **54**, 2473–2483.

Chung, S. L. & Sun, S.-s. (1992). A new genetic model for the East Taiwan Ophiolite and its implications for Dupal domain in the northern hemisphere. *Earth and Planetary Science Letters* **109**, 133–145.

Chung, S. L., Sun, S.-s., Tu, K., Chen, C.-H. & Lee, C. Y. (1994). Late Cenozoic basaltic volcanism around the Taiwan Strait, SE China: product of lithosphere–asthenosphere interaction during continental extension. *Chemical Geology* **112**, 1–20.

Chung, S. L., Jahn, B. M., Chen, S., Lee, T. & Chen, C.-H. (1995*a*). Miocene basalts in northwestern Taiwan: evidence for EM-type mantle sources in the continental lithosphere. *Geochimica et Cosmochimica Acta* **59**, 549–555.

Chung, S. L., Yang, T. F., Lee, C. Y. & Chen, C.-H. (1995*b*). The igneous provinciality in Taiwan: consequence of continental rifting superimposed by Luzon and Ryukyu subduction systems. *Journal of Southeast Asian Earth Sciences* **11**, 73–80.

Chung, S. L., Wang, S. L., Shinjo, R., Lee, C. S. & Chen, C.-H. (2000). Initiation of arc magmatism in an embryonic continental rifting zone of the southernmost part of Okinawa Trough. *Terra Nova* **12**, 225–230.

Chung, S. L., Sun, S.-s. & Crawford, A. J. (2001*a*). Indian Ocean type convecting mantle underlies East Asia: a consequence of Gondwana breakup and reassembly? *Western Pacific Earth Sciences* **1**, 1–18.

Chung, S. L., Wang, K. L., Crawford, A. J., Kamenetsky, V. S., Chen, C.-H., Lan, C. Y. & Chen, C. H. (2001*b*). High-Mg potassic rocks from Taiwan: implication for the genesis of orogenic potassic magmas. *Lithos* **59**, 153–170.

Crawford, A. J., Falloon, T. J. & Eggins, S. (1987). The origin of island arc high-alumina basalts. *Contributions to Mineralogy and Petrology* **97**, 417–430.

Davies, J. H. & von Blankenburg, F. (1995). Slab breakoff: a model of lithospheric detachment and its test in the magmatism and deformation of collisional orogens. *Earth and Planetary Science Letters* **129**, 85–102.

Dewey, J. F. (1988). Extensional collapse of orogens. *Tectonics* **7**, 1123–1139.

Eguchi, T. & Uyeda, S. (1983). Seismotectonics of the Okinawa Trough and Ryukyu Arc. *Memoir of the Geological Society of China* **5**, 189–210.

Foley, S. F., Venturelli, G., Green, D. H. & Toscani, L. (1987). The ultrapotassic rocks: characteristics, classification, and constraints for petrogenetic models. *Earth-Science Reviews* **24**, 81–134.

Galer, S. J. G. & Abouchami, W. (1998). Practical application of lead triple spiking for correction of instrumental mass discrimination. *Mineralogical Magazine* **62A**, 491–492.

Gaetani, G. A., Grove, T. L. & Bryan, W. B. (1993). The influence of water on the petrogenesis of subduction-related igneous rocks. *Nature* **365**, 332–335.

Gerstenberger, H. & Haase, G. (1997). A highly effective emitter substance for mass spectrometric Pb isotope ratio determinations. *Chemical Geology* **136**, 309–312.

Gill, J. B. (1981). *Orogenic Andesites and Plate Tectonics*. Berlin: Springer, 390 pp.

Govindaraju, K. (1994). 1994 compilation of working values and sample description for 383 geostandards. *Geostandards Newsletter* **18**, 1–158.

Halliday, A. N., Lee, D. C., Tommasini, S., Davies, G. R., Paslick, C. R., Fitton, J. G. & James, D. E. (1995). Incompatible trace elements in OIB and MORB and source enrichment in the sub-oceanic mantle. *Earth and Planetary Science Letters* **133**, 379–395.

Harris, N. B. W., Pearce, J. A. & Tindle, A. G. (1986). Geochemical characteristics of collision zone magmatism. In: Coward, M. P. & Ries, A. C. (eds) *Collision Tectonics. Geological Society, London, Special Publications* **19**, 67–82.

Hart, S. R. (1984). A large-scale isotope anomaly in the southern hemisphere. *Nature* **309**, 753–757.

Hart, S. R. (1988). Heterogeneous mantle domains: signatures, genesis and mixing chronologies. *Earth and Planetary Science Letters* **90**, 273–296.

Houseman, G. A., McKenzie, D. P. & Molnar, P. J. (1981). Convective instability of a thickened boundary layer and its relevance for the thermal evolution of continental convergent belts. *Journal of Geophysical Research* **86**, 6115–6132.

Hsiao, L. Y., Lin, K. A., Huang, S. T. & Teng, L. S. (1998). Structural characteristics of the southern Taiwan–Sinzi Folded Zone. *Petroleum Geology of Taiwan* **32**, 133–153 (in Chinese).

Jahn, B. M. (1986). Mid-ocean ridge or marginal basin origin of the East Taiwan Ophiolite: chemical and isotopic evidence. *Contributions to Mineralogy and Petrology* **92**, 194–206.

Johnson, K. T. M. (1998). Experimental determination of partition coefficients for rare earth and high-field-strength elements between clinopyroxene, garnet, and basaltic melt at high pressures. *Contributions to Mineralogy and Petrology* **133**, 60–68.

Juang, W. S. (1988). Geochronology and chemical variations of late Cenozoic volcanic rocks in Taiwan. Ph.D. thesis, National Taiwan University, Taipei, 231 pp. (in Chinese).

Juang, W. S. (1993). Diversity and origin of Quaternary basaltic magma series in northern Taiwan. *Bulletin of the National Museum of Natural Science* **4**, 125–166.

Kamata, H. & Kodama, K. (1994). Tectonics of an arc–arc junction: an example from Kyushu Island at the junction of the Southwest Japan Arc and the Ryukyu Arc. *Tectonophysics* **233**, 69–81.

Kao, H., Shen, S. J. & Ma, K. F. (1998). Transition from oblique subduction to collision: earthquakes in the southwesternmost Ryukyu arc–Taiwan region. *Journal of Geophysical Research* **103**, 7211–7229.

Kelemen, P. B., Shimizu, N. & Dunn, T. (1993). Relative depletion of niobium in some arc magmas and the continental crust: partitioning of K, Nb, La and Ce during melt/rock reaction in the upper mantle. *Earth and Planetary Science Letters* **120**, 111–134.

Keppler, H. (1996). Constraints from partitioning experiments on the compositions of subduction-zone fluids. *Nature* **380**, 237–240.

Kong, F., Lawver, L. A. & Lee, T.-Y. (2000). Evolution of the southern Taiwan–Sinzin Folded Zone and opening of the southern Okinawa trough. *Journal of Asian Earth Sciences* **18**, 325–341.

Lan, C. Y., Lee, T. & Wang Lee, C. (1990). The Rb–Sr isotopic record in Taiwan gneisses and its tectonic implication. *Tectonophysics* **183**, 129–143.

Lee, C. T. & Wang, Y. (1988). Quaternary stress changes in northern Taiwan and their tectonic significance. *Proceedings of the Geological Society of China* **31**, 154–168.

Lee, C. Y., Tsai, J. H., Ho, H. H., Yang, T. F., Chung, S. L. & Chen, C.-H. (1997). Quantitative analysis in rock samples by an X-ray fluorescence spectrometer (I) major elements. *Program with Abstracts of 1997 Annual Meeting of Geological Society of China, Taipei*, pp. 418–420 (in Chinese).

Lee, S. F. (1996). Volcanic sequence study of the Tatun Volcano Group: the Chihsinshan subgroup. M.S. thesis, National Taiwan University, Taipei, 136 pp. (in Chinese).

Letouzey, J. & Kimura, M. (1986). The Okinawa Trough: genesis of a back-arc basin developing along a continental margin. *Tectonophysics* **125**, 209–230.

Li, X. H. (1997). Geochemistry of the Longsheng Ophiolite from the southern margin of Yangtze Craton, SE China. *Geochemical Journal* **31**, 323–337.

Liu, C. C. (1995). The Ilan plan and the southwestward extending Okinawa Trough. *Journal of the Geological Society of China* **38**, 229–242.

Liu, T. K. (1987). Some new radiometric ages of rocks from Taiwan. *Program and Abstract Volume, Annual Meeting of Geological Society of China*, p. 62.

Liu, T. K., Chen, C.-H. & Jiang, S. H. (1986). Fission-track study of igneous rocks from northern Taiwan. Unpublished report to the National Science Council, Taiwan, 7 pp.

Liu, Y., Liu, H. & Li, X. H. (1996). Simultaneous and precise determination of 40 trace elements in rock samples. *Geochimica* **25**, 552–558 (in Chinese).

Lonergan, I. & White, N. (1996). Origin of the Betic–Rif mountain belt. *Tectonics* **16**, 504–522.

Maaloe, S. (1994). Estimation of the degree of partial melting using concentration ratios. *Geochimica et Cosmochimica Acta* **58**, 2519–2525.

Maheo, G., Guillot, S., Blichert-Toft, J., Rolland, Y. & Pecher, A. (2002). A slab breakoff model for the Neogene thermal evolution of South Karakorum and South Tibet. *Earth and Planetary Science Letters* **195**, 45–58.

Malavielle, J. (1993). Late orogenic extension in mountain belts: insights from the Basin and Range and the late Paleozoic Variscan belt. *Tectonics* **12**, 1115–1130.

Maury, R. C., Defant, M. J. & Joron, J.-L. (1992). Metasomatism of the sub-arc mantle inferred from trace elements in Philippine xenoliths. *Nature* **360**, 661–663.

Michard, A., Gurriet, P., Soudant, M. & Albarède, F. (1985). Nd isotope in French Phanerozoic shales: external vs. internal aspects of crustal evolution. *Geochimica et Cosmochimica Acta* **49**, 601–610.

Middlemost, E. A. K. (1975). The basalt clan. *Earth-Science Reviews* **11**, 337–364.

Miki, M. (1995). Two-phase opening model for the Okinawa Trough inferred from paleomagnetic study of the Ryukyu Arc. *Journal of Geophysical Research* **100**, 8169–8184.

Myers, J. D., Frost, C. & Angevine, C. L. (1986). A test of a quartz eclogite source for parental Aleutian magmas: a mass balance approach. *Journal of Geology* **94**, 811–828.

Park, J.-O. (1996). Seismic stratigraphy and tectonic evolution of the southern Ryukyu island arc. Ph.D. thesis, Ocean Research Institute, University of Tokyo, 145 pp.

Pearce, J. A. & Parkinson, I. J. (1993). Trace element models for mantle melting: application to volcanic arc petrogenesis. In: Prichard, H. M., Alabaster, T., Harris, N. B. W. & Neary, C. R. (eds) *Magmatic Processes and Plate Tectonics. Geological Society, London, Special Publications* **76**, 373–403.

Pearce, J. A. & Peate, D. W. (1995). Tectonic implications of the composition of volcanic arc magmas. *Annual Review of Earth and Planetary Sciences* **23**, 251–285.

Pearce, J. A., Bender, J. F., De Long, S. E., Kidd, W. S. F., Low, P. J., Güner, Y., Saroglu, F., Yilmaz, Y., Moorbath, S. & Mitchell, J. G. (1990). Genesis of collision volcanism in Eastern Anatolia, Turkey. *Journal of Volcanology and Geothermal Research* **44**, 189–229.

Pearce, J. A., Baker, P. E., Harvey, P. K. & Luff, I. W. (1995). Geochemical evidence for subduction fluxed mantle melting and fractional crystallization beneath the South Sandwich Island arc. *Journal of Petrology* **36**, 1073–1109.

Platt, J. P. & England, P. C. (1993). Convective removal of lithosphere beneath mountain belts: thermal and mechanical consequences. *American Journal of Science* **293**, 307–336.

Platt, J. P. & Visser, R. L. M. (1989). Extensional collapse of thickened continental lithosphere: a working hypothesis for the Alboran Sea and Gibraltar arc. *Geology* **17**, 540–543.

Roeder, P. L. & Emslie, R. F. (1970). Olivine–liquid equilibrium. *Contributions to Mineralogy and Petrology* **29**, 275–289.

Sadeghi, H., Suzuki, S. & Takenaka, H. (2000). Tomographic low-velocity anomalies in the uppermost mantle around the northeastern edge of Okinawa trough, the backarc of Kyushu. *Geophysical Research Letters* **27**, 277–280.

Schmidt, K. H., Bottazzi, P., Vannucci, R. & Mengel, K. (1999). Trace element partitioning between phlogopite, clinopyroxene and leucite lamproite melt. *Earth and Planetary Science Letters* **168**, 287–299.

Shinjo, R. (1998). Petrochemistry and tectonic significance of the emerged late Cenozoic basalts behind the Okinawa Trough–Ryukyu arc system. *Journal of Volcanology and Geothermal Research* **80**, 39–53.

Shinjo, R. (1999). Geochemistry of high Mg andesites reflects the tectonic evolution of the Okinawa Trough–Ryukyu arc system. *Chemical Geology* **157**, 69–88.

Shinjo, R., Ban, M., Saito, K. & Kato, Y. (1991). K–Ar dating of the volcanic rocks in the Ryukyu arc. *Journal of the Japanese Association of Mineralogists, Petrologists and Economic Geologists* **86**, 323–328 (in Japanese).

Shinjo, R., Chung, S. L., Kato, Y. & Kimura, M. (1999). Geochemical and Sr–Nd isotopic characteristics of volcanic rocks from the Okinawa Trough and Ryukyu arc: implications for the evolution of a young, intra-continental backarc basin. *Journal of Geophysical Research* **104**, 10591–10608.

Sibuet, J.-C., Hsu, S.-K., Shyu, C.-T. & Liu, C.-S. (1995). Structural and kinematic evolutions of the Okinawa Trough backarc basin. In: Taylor, B. (eds) *Backarc Basins: Tectonics and Magmatism*. New York: Plenum, pp. 343–379.

Sibuet, J.-C., Deffontaines, B., Hsu, S.-K., Thareau, N., Le Formal, J.-P., Liu, C. S. & the ACT party (1998). The Okinawa Trough backarc basin: early tectonic and magmatic evolution. *Journal of Geophysical Research* **103**, 30245–30267.

Sun, S. C. & Hsu, Y. Y. (1991). Overview of the Cenozoic geology and tectonic development of offshore and onshore Taiwan. *TAICRUST Workshop Proceedings (June 10–12, 1991), Taipei, Taiwan*, pp. 35–47.

Sun, S.-s. (1980). Lead isotopic study of young volcanic rocks from mid-ocean ridges, ocean islands and island arcs. *Philosophical Transactions of Royal Society of London, Series A* **297**, 409–445.

Sun, S.-s. & McDonough, W. F. (1989). Chemical and isotopic systematics of oceanic basalts: implications for mantle composition and processes. In: Saunders, A. D. & Norry, M. J. (eds) *Magmatism in the Ocean Basins. Geological Society, London, Special Publications* **42**, 313–345.

Sun, S.-s., Nesbitt, R. W. & Sharaskin, A. Y. (1979). Geochemical characteristics of mid-ocean ridge basalts. *Earth and Planetary Science Letters* **44**, 119–138.

Suppe, J. (1984). Kinematics of arc–continent collision, flipping of subduction, and back-arc spreading near Taiwan. *Memoir of the Geological Society of China* **6**, 21–34.

Tatsumi, Y. & Kogiso, T. (1997). Trace element transport during dehydration processes in the subducted oceanic crust: 2. Origin of chemical and physical characteristics in arc magmatism. *Earth and Planetary Science Letters* **148**, 207–221.

Tatsumoto, M., Basu, A. R., Huang, W. K., Wang, J. W. & Xie, G. H. (1992). Sr, Nd, and Pb isotopes of ultramafic xenoliths in volcanic rocks of Eastern China: enriched components EMI and EMII in subcontinental lithosphere. *Earth and Planetary Science Letters* **113**, 107–128.

Taylor, R. N. & Nesbitt, R. W. (1998). Isotopic characteristics of subduction fluids in an intra-oceanic setting, Izu–Bonin Arc, Japan. *Earth and Planetary Science Letters* **164**, 79–98.

Teng, L. S. (1990). Geotectonic evolution of late Cenozoic arc–continent collision in Taiwan. *Tectonophysics* **183**, 57–76.

Teng, L. S. (1996). Extensional collapse of the northern Taiwan mountain belt. *Geology* **24**, 949–952.

Teng, L. S., Chen, C.-H., Wang, W. S., Liu, T. K., Juang, W. S. & Chen, J. C. (1992). Plate kinematic model for late Cenozoic arc magmatism in northern Taiwan. *Journal of the Geological Society of China* **35**, 1–18.

Thirlwall, M. F. (2000). Inter-laboratory and other errors in Pb isotope analyses investigated using a ^{207}Pb–^{204}Pb double spike. *Chemical Geology* **163**, 299–322.

Tsao, S. J. (1994). Potassium–argon age determination of volcanic rocks from the Tatun volcano group. *Bulletin of the Central Geological Survey* **9**, 137–154 (in Chinese).

Tu, K., Flower, M. J., Carlson, R. W., Xie, G., Chen, C. Y. & Zhang, M. (1992). Magmatism in the South China Basin 1. Isotopic and trace-element evidence for an endogenous Dupal mantle component. *Chemical Geology* **97**, 47–63.

Turner, S., Sandiford, M. & Foden, J. (1992). Some geodynamic and compositional constraints on 'postorogenic' magmatism. *Geology* **20**, 931–934.

Turner, S., Hawkesworth, C. J., Liu, J. Q., Rogers, N., Kelley, S. & van Calsteren, P. (1993). Timing of Tibetan uplift constrained by analysis of volcanic rocks. *Nature* **364**, 50–53.

Turner, S., Arnaud, N., Liu, J., Rogers, N., Hawkesworth, C., Harris, N., Kelley, S., van Calsteren, P. & Deng, W. (1996). Post-collisional, shoshonitic volcanism on the Tibetan Plateau: implications for convective thinning of the lithosphere and the source of ocean island basalts. *Journal of Petrology* **37**, 45–71.

Turner, S., Platt, J. P, George, R. M. M., Kelley, S. P., Pearson, D. G. & Nowell, G. M. (1999). Magmatism associated with orogenic collapse of the Betic–Alboran Domain, SE Spain. *Journal of Petrology* **40**, 1011–1036.

Wageman, J. M., Hilde, T. W. C. & Emery, K. O. (1970). Structure framework of East China Sea and Yellow Sea. *AAPG Bulletin* **54**, 1611–1643.

Wang, K. L., Chung, S. L., Shinjo, R., Chen, C. H., Yang, T. F. & Chen, C.-H. (1999). Post collisional magmatism around northern Taiwan and its relation with opening of the Okinawa Trough. *Tectonophysics* **308**, 363–376.

Wang, K. L., Chen, C. H., Chung, S. L., Lin, L. H., Lo, C. H., Yang, T. F. & Lee, H. Y. (2000). Field occurrence, $^{40}Ar/^{39}Ar$ dating and petrochemical features of volcanic rocks in Mienhuayu off NE Taiwan. *Journal of the Geological Society of China* **43**, 247–266.

Wang, K. L., Chung, S. L., Chen, C. H. & Chen, C.-H. (2002). Geochemical constraints on the petrogenesis of high-Mg basaltic andesites from the northern Taiwan volcanic zone and their geodynamic significance. *Chemical Geology* **182**, 513–528.

Wang, K. L., O'Reilly, S. Y., Griffin, W. L., Chung, S. L. & Pearson, N. J. (2003). Proterozoic mantle lithosphere beneath the extended margin of the South China Block: *in situ* Re–Os evidence. *Geology* **31**, 709–712.

Wang, S. L. (1998). Ar–Ar dating and geochemistry of volcanic rocks dredged from the middle Okinawa Trough. MS thesis, National Taiwan University, Taipei (in Chinese).

Wang, W. S. & Chen, C.-H. (1990). The volcanology and fission track age dating of pyroclastic deposits in Tatun Volcano group, northern Taiwan. *Acta Geologica Taiwanica* **28**, 1–30.

Woodhead, J. D., Volker, F. & McCulloch, M. T. (1995). Routine lead isotope determination using lead-207–lead-204 double spike: a long-term assessment of analytical precision and accuracy. *Analyst* **120**, 35–39.

Wyllie, P. J. & Sekine, T. (1982). The formation of mantle phlogopite in subduction zone hybridization. *Contributions to Mineralogy and Petrology* **79**, 375–380.

Yang, H. J., Chen, J. C. & Yang, H. Y. (1987). Geochemistry of ultramafic nodules in basaltic rocks from Peiliao, Penghu Islands and Liutsu, Northern Taiwan. *Proceedings of the Geological Society of China* **30**, 44–57.

Yeh, Y. H., Lin, C. H. & Roecker, S. W. (1989). A study of upper crustal structures beneath northeastern Taiwan: possible evidence of the western extension of Okinawa Trough. *Proceedings of the Geological Society of China* **32**, 139–156.

Yeh, Y. H., Barrier, E., Lin, C. H. & Angelier, J. (1991). Stress tensor analysis in the Taiwan area from focal mechanisms of earthquakes. *Tectonophysics* **200**, 267–280.

Yu, S. B. & Chen, H. Y. (1994). Global positioning system measurements of crustal deformation in the Taiwan arc–continent collision zone. *Terrestrial, Atmospheric and Oceanic Sciences* **5**, 477–498.